

## **BOREHOLE GEOLOGY AND HYDROTHERMAL ALTERATION MINERALOGY OF OW-807A, OLKARIA GEOTHERMAL FIELD**

**Danson Warui Kariuki**

Kenya Electricity Generating Company PLC

Olkaria Geothermal Project

P.O. Box 785 – 20117

Naivasha

KENYA

*DWarui@kengen.co.ke*

### **ABSTRACT**

OW-807A is a directional well (N 135°) drilled within the Southeast sector of the larger Olkaria Geothermal Field to a total depth of 2690 m b.g.l., with production casing set at 1004 m b.g.l. The well was drilled to appraise the potential of the area towards the Ol-Njorowa Gorge, where numerous dykes and volcanic centres have been identified. The study aims at providing a better understanding of the geothermal system encountered based on the lithostratigraphy relations, alteration mineralogy paragenesis and assemblages, and the permeability conditions characterising the well. OW-807A is characterised by six alteration zones based on the first occurrence of key index minerals such as zeolites, quartz, chlorite, epidote and actinolite. The uppermost sections of the well are marked by a rapid increase in prograde alteration and characterised by the shallow occurrence of chlorites, epidote and actinolite while the deeper sections represent a deep convective geothermal system. Determination of clay minerals show the changes in physical and chemical conditions of the circulating geothermal fluids with depth, represented by occurrence of smectites, mixed layer clays, illite and chlorites. A reversal in temperature is observed at a depth of 1100 m b.g.l. It is also observed in the precipitation of fluorite between 900 m to 1468 m b.g.l., imprinting higher temperature minerals. The reversal is associated with the well intersecting a series of NE-SW trending faults at depth, associated with the Ol Njorowa Gorge. The targeted dyke systems and intrusives show minimal contribution to the overall thermal regime of the well and are considered to have gradually cooled with time.

### **1. INTRODUCTION**

This report forms an important part of the six-month GRÓ GTP training of the author in 2021 in Borehole Geology. The programme entailed training on the identification and determination of rock types through logging of the geothermal well cuttings and analysis of thin sections, X-Ray Diffraction and Scanning Electron Microscope analysis for clay minerals. Training on the interpretation of the different lithological, geophysical and temperature logs was also undertaken. However, only temperature logs have been incorporated into this study due to data availability. The project work entailed the selection of a well, in this case OW-807A within the Olkaria Geothermal Field, with the aim to characterise the lithostratigraphy, alteration mineralogy, mineral sequences and relations, through

which the knowledge on the geothermal system can be improved, thus enhancing decision making for development purposes. To achieve these objectives, the different analytical techniques learnt during the training programme were applied. This report thus provides a detailed analysis of all the geological data obtained using the different techniques and equipment, and integration and interpretation to determine the geothermal system characteristics of the well and their changes with time when observed.

The occurrence of geothermal resources in Olkaria is associated with the Kenyan Rift system, forming part of the larger East African Rift System (EARS), a 5000 km long series of fault bordered depressions straddling East Africa in a roughly N-S direction, marking a divergent boundary between two major plates, the Somalian and the Nubian Plates (Chorowicz, 2005).

The geothermal resource potential in Kenya has been estimated to be 10,000 MWe, associated with the occurrence of over 14 geothermal areas (Figure 1) of which three, Olkaria, Menengai and Paka fields, are in different stages of development while the others are still in the exploration phase. Geothermal exploration efforts in the Kenyan Rift started in the 1950's, spearheaded both by the Kenyan government and international development partners, culminating in the drilling of the first wells in the Olkaria field located within the central segment, albeit unsuccessfully. Continued improvements on both the scientific knowledge, technology and data processing capabilities have greatly improved the development of the geothermal conceptual models leading to better well siting, drilling, casing programs and testing of geothermal wells over time. To date, over 300 geothermal wells have been drilled in the Olkaria Geothermal Field, including production, hot and cold re-injection, and makeup wells, signifying the importance of proper and correct conceptual models.

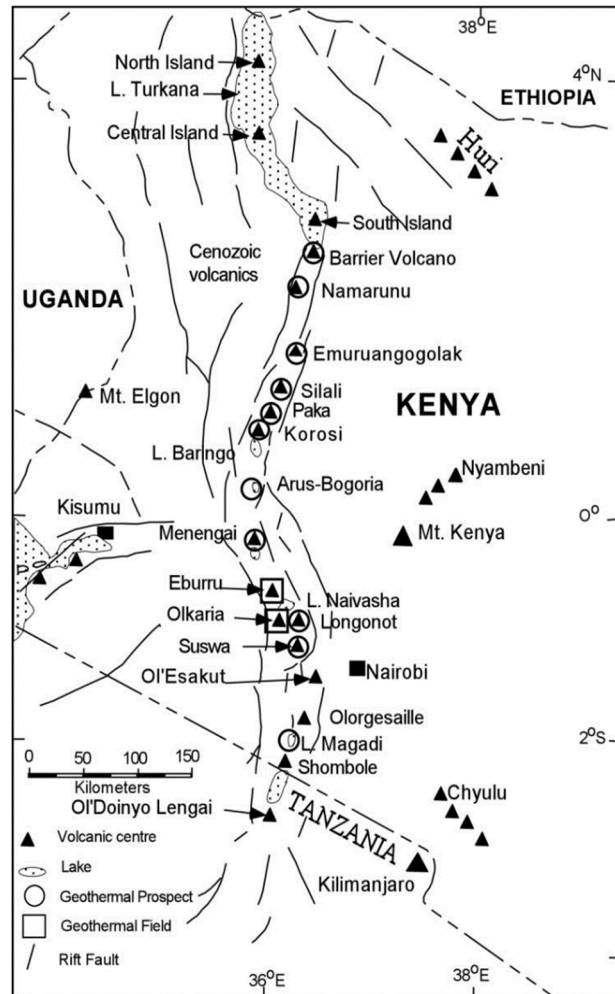


FIGURE 1: Geothermal areas in the Kenyan Rift system (Lagat, 2004)

The Olkaria Geothermal Field currently supports a generation capacity of 865 MWe, but the field has been subdivided into seven sectors (Figure 2) for ease of management. These areas include the Olkaria-East, North-East, North-West, South-East, West, Central and the Domes sectors. The Olkaria West field is operated by OrPower Inc, an independent power producer, while the rest of the fields are operated by KenGen PLC.

The Olkaria South-East Field is poised for development of the proposed 140 MWe Olkaria VI power plant through a Public Private Partnership model. To attain the necessary steam requirements, several wells have been drilled, mainly to assess the reservoir conditions and appraise the field, with varying success rates. To enhance decision making on future location of wells, within this sub-field, it is necessary to characterize the evolution history of the geothermal system in the area. Accurate determinations of the changes through time in terms of temperature, fluid composition, water-rock interactions, and permeability aspects controlling fluid flow within the system are important, as they contribute greatly to the geological conceptual model of the area. The determinations through the study of alteration mineral assemblages, including clays, mineral paragenesis provide insights into the thermal

regimes, permeability distribution and fluid flow regimes that have occurred within the system over time.

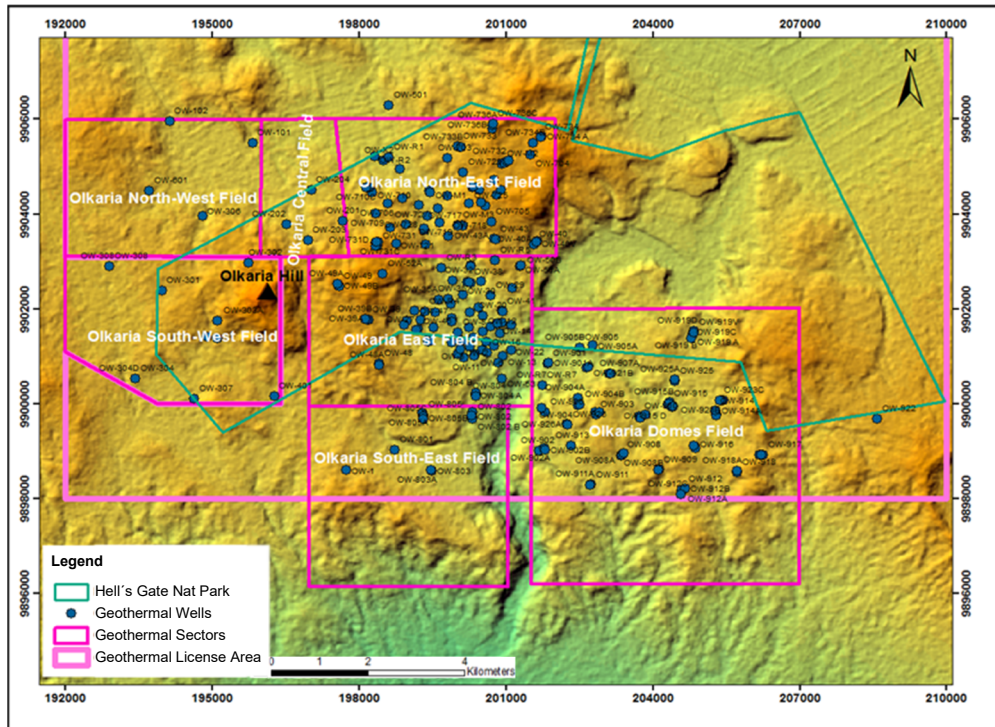


FIGURE 2: Geothermal development sectors within the Olkaria Field (Muchemi, 2000; modified by Otieno, 2016)

The present study encompasses a detailed analysis of the lithology and alteration mineralogy for geothermal well cuttings of well OW-807A, located within the Olkaria Geothermal Field. Four methods were employed for the study, which is binocular microscope analysis of the rock cuttings, polarizing microscope analysis of thin sections, X-ray diffraction of samples from selected depths and Scanning Electron Microscope analysis for the identification and characterization of clays and their compositional data. The outcome of the study will be integrated into the conceptual model of the Olkaria Geothermal System and are expected to improve future drill sites selection and well targeting, improve casing designs, and generally support the basis for future development plans within the study area.

## 2. GEOLOGICAL SETTING

### 2.1 Regional geological setting

The EARS, a classical continental rift, is characterised by extensive volcanic activity which has progressed southwards, commencing in the north about 45 Ma ago progressing towards Tanzania in the south about 8 Ma ago. The activity is largely driven by the presence of two mantle plumes, namely the Kenyan plume, and the Afar plume, based on topographic and gravity data and supported by radiogenic isotope studies (Ebinger et al., 1989). Based on the characteristics of the radiogenic isotopes and the results of seismic tomography, it has been deduced that the Afar plume has a deep origin in an undegassed part of the mantle, whereas the Kenyan plume is inferred to have a shallow origin and is older (Rogers et al., 2000). According to Gordon and Judy (1986) and Rogers et al. (2000), the African plate has drifted north-eastward at a rate of 1-3 cm/yr over the past 50 Ma which is close to 1000 km, further supporting the conclusion that the Kenyan plume is older. Smith and Mosley (1993) deduced in

their studies that the lithosphere exerts strong controls on the location, volume, and composition of magmatism in East Africa, resulting in a more complex mechanism due to the lack of one-to-one correlation between plate motion, magmatism and volcanism trend.

The Kenyan segment of the EARS has been the subject of numerous geophysical studies that have contributed immensely to the understanding of the lithospheric structure. Based on these studies, the crustal thickness has been deduced to be 30 km beneath the graben valley at latitude 0.5°, 40 km in the western flank, and 35 km in the eastern flank, with normal faults, tilted blocks and rollover structures expressing the rift asymmetry (Achauer et al., 1992; Chorowicz, 2005). The evolution of the Kenyan rift volcanism is comprised several periods, with the formation of the graben basins and horsts uplift commencing at 11-5.3 Ma, formation of the Kerio valley between 5.3 and 1.6 Ma, and concentration of volcanic activity in the eastern part of the northern rift and central segment between 1.6-0.01 Ma. Normal faults are the main tectonic features, interpreted to be listric when they connect at depth with low angle antithetic faults (Hackman et al., 1990; Smith and Mosley, 1993).

Major faults on the western side developed between 12 and 7 Ma, dipping east-north-east (Strecker et al., 1990). Antithetic faulting followed on west and west-south-west dipping normal faults, resulting in the formation of a full graben, later being cut by younger west dipping faults. A subsidence phase then occurred in the central depression before the eruption of voluminous trachytes between 1.9 and 0.4 Ma while development of normal faults striking north-north-west continued after the eruptions. Older north-north-west striking faults were also re-activated with considerable dextral components of movement, with the youngest displacements showing clockwise rotation of the stress field (Strecker et al., 1990).

The area to the north and south of Lake Naivasha is characterised by the occurrence of closely spaced faults with throws of <150 m, associated with the east-west extension. Their probable presence is, furthermore, postulated within the area around the lake, though their exposure is masked by younger volcanic and sedimentary units (Baker et al., 1988).

## 2.2 Local geological setting of the project area

The Greater Olkaria Volcanic Complex (GOVC) is a multicentred volcanic field covering an area of 240 km<sup>2</sup>. At least 80 smaller volcanic centres have formed within it, mostly occurring as either steep sided domes, formed of lava and/or pyroclastic rocks, or as thick comendite lava flows of restricted lateral extent. Petrographically, the comendites are commonly characterised by quartz, sanidine, riebeckite or arfvedsonite, and rare aenigmatite, hornblende and aegirine phenocrysts, though not all phases are compatible, in a fine to medium grained matrix containing quartz and Fe-Ti oxides (Macdonald et al., 1987).

The comendites have likely formed by volatile induced crustal anatexis (Macdonald and Scaillet, 2006). These rhyolite flows are blanketed by thick fall deposits originating from Olkaria, Longonot and probably Suswa Volcano (Clarke et al., 1990; Omenda, 1998), except for the Ololbutot lava flow dated at 180 ± 50 yr. BP (Macdonald and Scaillet, 2006), which represents the most recent volcanic activity within the complex (Clarke et al., 1990).

The subsurface geology has been categorised into four distinct groups based on age, tectono-stratigraphy, composition and stratigraphic position of the lithological units. These are The Upper Olkaria Volcanics, Olkaria Basalts, the Plateau Trachytes, and the Mau Tuffs

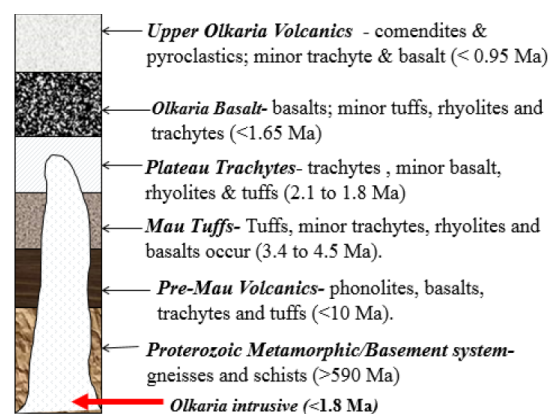


FIGURE 3: Lithostratigraphy of the GOVC area (modified from Omenda, 1998)



## 2.4 Overview of well OW-807A

OW-807A is a directional well (azimuth N 135°) drilled to a total depth of 2690 m below ground level (m b.g.l.) and referenced by UTM coordinates N:9899580.653 m, E:200613.761 m at an elevation of 1898 metres above mean sea level (m a.s.l.) as shown in Figure 5. The well was intended to provide steam to the proposed Olkaria VI geothermal power plant. The drilling of this well towards the southeast was to intersect a series of N-S and NE-SW trending dykes and volcanic plugs in the Ol Njorowa Gorge, with the purpose of evaluating their potential as heat sources.

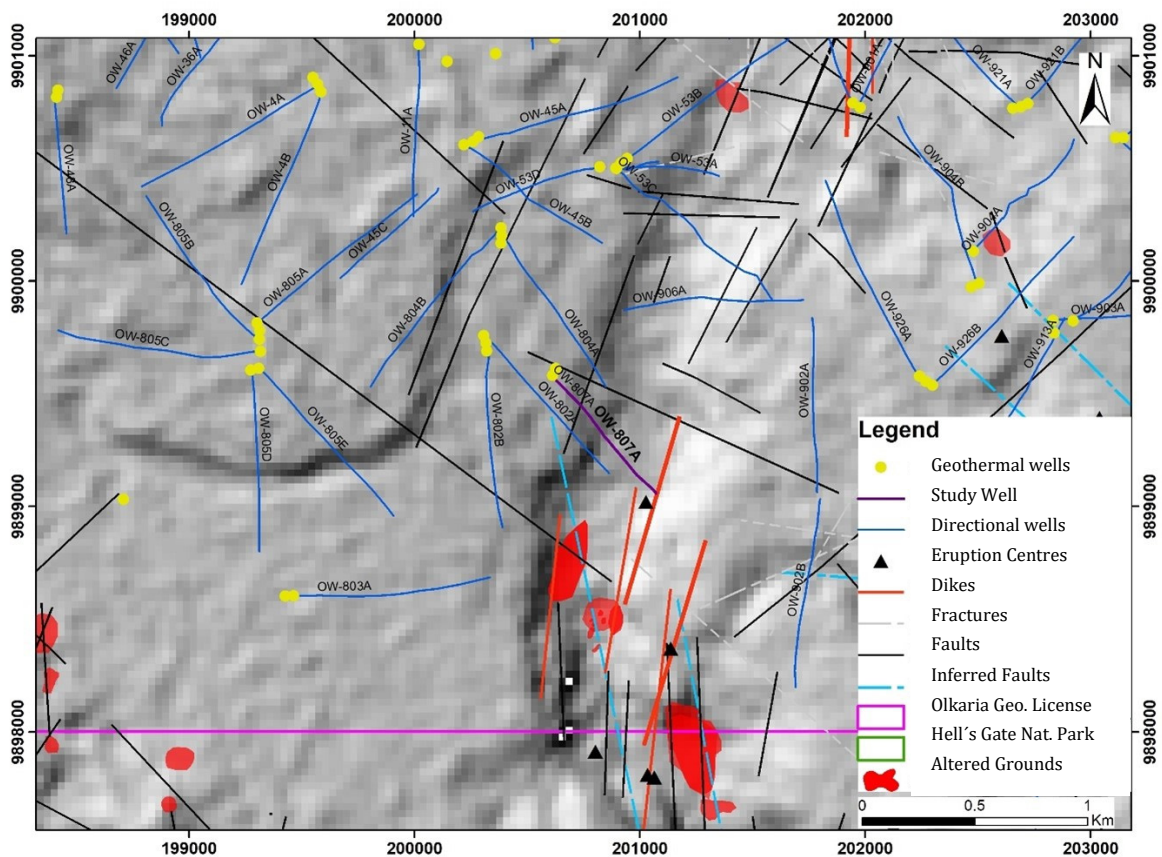


FIGURE 5: Location map of well OW 807A

## 2.5 Drilling program

The OW-807A well was drilled for a total of 117 days, with a 9 5/8 " production casing set at 1004 m below cellar top (CT). The plot in Figure 6 shows the progress of the drilling activities with a break in the drilling activities necessitated by a rig change. A summary of the drilling timeline is presented below.

- Phase I:** Drilling of the 26" hole to a depth of 58 m below CT and installation of a 20" surface casing and cementing activities took a total of 3 days. No drilling challenges were experienced within this depth.
- Phase II:** This involved the drilling of the well from 58 m below CT to 302 m below CT with a 17½" drill bit for the 13⅜" anchor casing and cementing activities that took a total of 13 days to complete. No major challenges were experienced.

- Phase III:** This involved the drilling of the well with a 12¼” bit to a depth of 1004 m below CT, setting of the 9<sup>5</sup>/<sub>8</sub>” production casing and cementing. This took a total of 24 days with no major drilling challenges encountered.
- Phase IV:** Drilling of this section with an 8½” drill bit to the terminal depth of 2690 m below CT and the running in hole of the 7” perforated liner took a total of 78 days. Drilling challenges encountered were instances of lost circulation, stuck drill pipe and fishing of drilling bit cones.

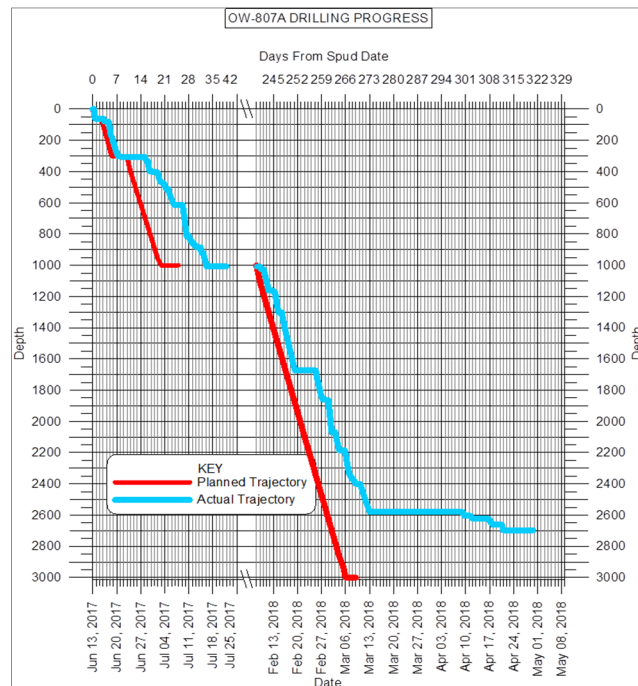


FIGURE 6: Drilling progress plot for well OW-807A

### 3. METHODOLOGY

#### 3.1 Binocular microscope analysis

Analysis of the OW-807A samples was carried out with an Olympus SZX 16 binocular microscope. The aim of the analysis was to determine the rock type(s), textures, alteration type, intensity and rank, mineral sequences and relations, and permeability conditions within the well.

For the analysis, the samples were rinsed thoroughly with water to remove unrelated drilling additives, placed in a petri-dish with water and mounted on the Loupe stage for analysis.

#### 3.2 Petrographic microscope analysis

The analysis involved the use of a polarising microscope to study thin sections prepared from selected geothermal well rock cuttings. To undertake the analysis, the samples are cut and glued on glass slides using a bonding compound and polished down to a thickness of approximately 30 µm. The analysis carried out involved the determination of the rock type by identification of the primary minerals through their optical characteristics and the evolution of the geothermal system through time by analyses of hydrothermal minerals. A total of 12 thin sections was analysed using a Leica DM 2700P Polarising microscope, fitted with an imaging station at the ISOR laboratory.

#### 3.3 X-Ray diffraction analysis

X-ray diffraction analysis of clay minerals was carried out on selected samples. After careful washing of the rock cuttings samples with distilled water, about 2 g of the sample is scooped into a glass test-tube. The tube is then filled with distilled water and put in a mechanical shaker for about four hours. The suspended clay-slurry is left to settle for about 10 minutes and then transferred onto a glass-slide, using a pipette. The sample is left to dry at ambient temperature and humidity. The sample is analysed after complete drying (UNT = untreated) and after measurement the sample is placed inside a closed desiccator, above a container filled with ethylene-glycol. The sample is left in the ethylene-glycol fume for 24 hours and then analysed (GLY = glycolated). Finally, the sample is heated in a furnace for about 1 hour in 550°C and after cooling, analysed again (HIT, heated).

Each sample is measured from  $2\theta = 2^\circ$ – $14^\circ$ , in  $0.02^\circ$  increments (steps) and measured for 1 second during each step. The set-up is saved to a parameter file *leir-a.dql*. Each measurement takes about 20 minutes. The X-ray beam is confined using  $0.5^\circ$  divergence and receiving slits. The equipment used is a Bruker AXS D8 Focus, producing Cu K- $\alpha$  radiation with  $1.54 \text{ \AA}$  wavelength at 40 kV and 40 mA. The detector used is a NaI scintillation counter. The set of three measurements is then viewed superimposed using special software for X-ray diffraction data display (Bruker, Diffra. Eva) where the peaks are compared to a well-established database, from the International Centre for Diffraction Data, for analysis.

### 3.4 Electron microprobe analysis

The Electron Microprobe Analysis (EMPA) is a technique for chemically analysing small, selected areas of solid samples in which x-rays are excited by a focused electron beam. Characteristic lines of the elements in the x-ray spectrum allow for a qualitative analysis while comparisons of intensities with those emitted from standard samples allow for a quantitative estimation of their concentrations with high accuracy and low detection limits under normal conditions. The spreading of the beam within the sample limits the spatial resolution to  $1 \mu\text{m}$  and the spatial distribution of specific elements recorded in the form of line profiles or two-dimensional maps are commonly displayed using a false colour scale. The instrumentation includes an electron source, electron lenses to focus the beam, beam deflection coils and electron detector to enable production of a scanning image, a vacuum system, specimen stage and an optical microscope (Reed, 2005).

For this study, a JEOL JXA-8230 Super probe was used with an accelerating voltage of 15kV, a current of 10 nA, an acquisition time of 120 s and a beam of  $10 \mu\text{m}$ . Four thin sections were carbon coated for the analysis but due to time constraints, only three of the four thin sections were analysed. The composition of selected grains, including their spectral data, elemental distribution maps and photomicrographs were acquired.

## 4. RESULTS

### 4.1 Lithostratigraphy

The lithological units, as determined from the analysis of the drill cuttings, have been categorised based on the stratigraphic units proposed by Omenda (1998) based on their stratigraphic position, age and composition. The lithology is comprised of pyroclastics and comenditic rhyolites which are the dominant units at shallow depth, followed by the underlying basalts, and the extensive Plateau Trachyte units and intrusives at the bottom as summarised in Table 1 below. The following section provides a detailed description of the units.

#### Pyroclastics

*Pyroclastics (0- 58 m)*: They are found at the surface, from 0-58 m and from 76-140 m, are grey to brownish in colour, and consist of heterogenous fragments of ashes, volcanic glass, pumice and rhyolitic fragments. Their provenance is mainly from Olkaria, but Longonot and Suswa volcano are also considered possible sources (Omenda, 1998). The unit is mainly oxidised due to interactions with atmospheric conditions.



TABLE 1: Summary of the lithology units in well OW-807A

Unit	Lithology Series	Depth Interval (m)	Thickness (m)	Lithology sub-series	Depth interval (m)	Loss zones (m)	Stratigraphic unit
1	Pyroclastics	0-140	122	Pyroclastics	0-58 76-140	150-302 326-346	Upper Olkaria Volcanics
2	Rhyolite	140-484	344	Rhyolite I	58-76		
				Rhyolitic tuff I	140-150		
				Rhyolite II	302-378		
				Trachyte I	378- 408		
				Basaltic tuff I	408- 444		
				Basalt I	440- 460		
				Rhyolite III	460-472		
				Rhyolitic tuff II	472-484		
3	Basalts	484-732	248	Basalt II	484-502		Olkaria Basalts
				Basaltic tuff II	502-508		
				Basalt III	508-516		
				Tuff I	516-564		
				Basalt IV	564-578		
				Tuff II	578-592		
				Basalt V with tuff intercalations	592-700		
				Rhyolite IV	700-732		
4	Trachytes	732-2130	1398	Trachytes II with rhyolites and tuffs	732-1044	946-950 1662-1682	Plateau Trachytes
				Tuff (breccia)	1044-1052	1786-1800 1852-1874	
				Trachyte III	1052-1170	1936-1950	
				Rhyolite V	1170-1250	1966-1994	
				Trachyte IV	1250-1462	1996-2018	
				Basalt VI	1462-1560	2044-2056	
				Rhyolite VI	1560-1698	2068-2096 2110-2130	
				Trachytes V with intrusions	1698-2130		
5	Intrusions	2130-2690	560	Micro-granite		2130-2690	Olkaria Intrusives

### Olkaria Rhyolites

*Rhyolites I (58 - 70 m):* Fine grained, moderately porphyritic rhyolite with numerous sanidine and quartz phenocrysts. The unit is massive and relatively fresh rock with instances of mild oxidation.

*Rhyolitic tuff I (140 - 150 m):* The rhyolitic tuffs are brownish to grey, fine grained, comprised of glassy tuffaceous fragments and crystalline rhyolitic lava fragments. The unit are altered to brownish clays, though the alteration intensity is low.

*Rhyolites II (302 - 378 m):* Whitish to pale grey, fine grained, slightly porphyritic rhyolite with minor quartz and sanidine phenocrysts. The unit appears glassy and shows minimal alteration of the glassy matrix to clays, while the feldspars are showing no changes associated with hydrothermal alteration. Oxidation is observed mostly within the rock matrix. Pyrite is common, and the rock shows interstitial porosity. Common alteration minerals are chalcedony and clays, indicative of the low temperature fluids circulating within this formation.

*Trachyte I (378 - 408 m):* Grey, fine grained, slightly porphyritic trachyte with sanidine in groundmass forming a distinctive flow texture. This unit is slightly altered to clays, mainly infilling vesicles and

fractures. Feldspars within the rock show the commencement of alteration to clays, while pyrite and oxides infilling veins and vesicles are also common.

*Trachytic tuff I (408 - 416 m)*: The trachytic tuff is pale green in colour, consisting of fine-grained heterogenous fragments of glassy tuff and lithic fragments of crystalline trachytic lava fragments. The tuff shows moderate to high alteration to clays, with secondary quartz infilling vesicles and pyrite mainly observed as matrix disseminations.

*Basalt I (416 - 436 m)*: Dark grey, fine-grained basalt, which is vesicular, slightly porphyritic with phenocrysts of plagioclase feldspars, augite and Fe-Ti oxides. The basalt is moderately altered to clays and is characterised by the occurrence of veins infilled with clays, calcite and quartz as secondary alteration minerals. The unit is characterised by secondary porosity associated with fractures and veins.

*Tuff (Breccia) I (436 - 440 m)*: The tuff/breccia is characterised by glassy fragments and forms a thin intercalated layer between successive basaltic lava flows.

*Basalt II (440 - 460 m)*: Dark grey basalt which is massive, fine grained and moderately porphyritic with plagioclase feldspar, augite and Fe-Ti oxides as phenocrysts. The unit is moderately altered unit with the feldspars showing advanced alteration. Augite is observed to alter to clays within the crystal with the outer edges rimmed by oxides.

*Rhyolite III (460 - 472 m)*: Light grey, fine grained rhyolite which is slightly porphyritic with distinct quartz phenocrysts. It has a spherulitic texture caused by the intergrowth of quartz and feldspar minerals and discernible primary amphiboles. The unit is slightly to moderately altered to clays, with fracture surfaces being covered by euhedral crystals of pyrite and chalcopyrite.

*Rhyolitic tuff II (472 - 484 m)*: Light green rhyolitic tuff which is fine grained and heterogenous comprising of rhyolitic lava fragments and minor glassy tuff. The unit shows moderate alteration to clays, with pyrite mainly disseminated in the rock matrix and fractures infilled by oxides.

### **Olkaria Basalts**

*Basalt III (484 - 502 m)*: Dark grey basalt which is slightly vesicular, fine grained and moderately porphyritic with plagioclase feldspar phenocrysts. The basalt shows high alteration intensity into hydrothermal clays. Within the unit, the pyroxenes show high alteration with augite being completely replaced by clays. Common alteration minerals are clays from the alteration of feldspars and mafic minerals and secondary quartz infilling vesicles and fractures.

*Basaltic tuff I (502 - 508 m)*: Pale green to dark grey tuff which is fine grained and heterogenous with both glassy and crystalline basaltic lava fragments. The alteration intensity is moderate, with clays and replacement calcite being the most common alteration minerals.

*Basalt IV (508 - 516 m)*: Dark grey basalt which is fine grained, slightly porphyritic with mainly plagioclase phenocrysts. The alteration intensity is high and common alteration minerals are clays and calcite, with the unit being characterised by veins and fractures.

*Tuff II (516 - 534 m)*: Pale green homogenous tuff which is characterised by consolidated volcanic sediments, which are thought to signify a period of quiescence in the volcanic activity.

*Basaltic tuff II (534 - 564 m)*: Pale green to grey tuff which is fine grained and heterogenous characterised by lithic fragments of crystalline basalt (30%), and glassy tuff (70%). Alteration is high with the first appearance of epidote observed at 534 m. Other common alteration minerals are clays, quartz, and calcite. The relative abundance of pyrite indicates highly permeable conditions within this depth range.

*Basalt V with minor tuff intercalations (564 - 700 m):* Dark grey, fine-grained basalt which is slightly porphyritic with plagioclase feldspar, augite phenocrysts, and shows high alteration intensity. The feldspars within this unit have been pervasively altered to clays, with the pyroxenes also showing alteration to mainly clays. Replacement of iron-oxides by sphene is common. Other alteration minerals include actinolite whose first appearance was observed at 664 m, formed by alteration of the mafic minerals, calcite, prehnite (646 m) and secondary quartz. Pyrite, relatively abundance indicates a highly permeable zone as a result of secondary porosity attributed to veining.

*Rhyolite IV (700 - 732 m):* Pale grey to brownish rhyolite which is fine grained and moderately porphyritic with sanidine and quartz phenocrysts and a quartz rich groundmass. In a thin section in plane polarized light, riebeckite with its characteristic blue colour is observed. The unit is massive with slight alteration and the feldspars showing alteration to clays along cleavage traces. Mild oxidation is observed on the surface of the fragments together with veins, causing high permeability.

### **Plateau Trachytes**

*Trachyte II (732 - 1044 m) with rhyolites and tuff intercalations:* Fine grained, massive trachyte which is sparsely to moderately porphyritic with distinct sanidine feldspar phenocrysts with a trachytic texture as a result of the arrangement of feldspar microlites in the rock matrix. Alteration intensity changes from slight in the upper part of the unit to highly altered with depth. Clays and epidote are often observed as an alteration of felsic minerals while chlorite clays, sphene, and actinolite have replaced the pyroxene. A minor, relatively fresh rhyolitic dyke is observed at 870-880 m depth which has led to an increase in alteration and oxidation in the units lying underneath and above this trachyte.

*Tuff (breccia) II (1044 - 1052 m):* Light green to grey tuffaceous breccia which is heterogenous with composite lithic fragments of crystalline trachytic lava and glassy tuff material. The tuff is highly altered to clays and shows mild oxidation on some of the lava fragments.

*Trachyte III (1052 - 1170 m) with minor tuffs:* The unit is characterised by fine grained, sparsely to moderately porphyritic trachyte with sanidine phenocrysts. The unit varies from dense to slightly vesicular, showing moderate to high alteration intensities. The amygdales are filled by clay and oxides as infillings. Pyrite disseminations, vein filling and oxidation are common within this zone, while calcite is observed at depths of 1098-1122 m. Permeability associated with secondary porosity in the form of veins is high within this unit.

*Rhyolite V (1170 - 1250 m):* The rhyolite is light grey to whitish in colour, fine grained, moderately porphyritic with quartz phenocrysts. The rhyolite is relatively fresh with minimal alteration. It is marked by a thin veneer of highly altered rhyolitic tuff (1170- 1178 m) overlying it.

*Trachyte IV (1250 - 1462 m):* The trachyte is fine grained, sparsely porphyritic with occasional sanidine phenocrysts and characteristic flow texture of feldspar microlites in the groundmass. The unit is massive and enhanced alteration of primary mineral phases into chlorite, epidote, prehnite, wollastonite and actinolite minerals common. Rock porosity is mainly secondary in the form of veins associated with fracturing of the rock.

*Basalt VI (1462 - 1560 m):* The basalt is dark grey, fine grained, slightly vesicular, moderately porphyritic with plagioclase feldspars, pyroxenes and Fe-Ti oxides. The unit shows high alteration intensity with the feldspars, epidote, and pyroxenes altering to clays and sphene replacing the oxides.

*Rhyolite VI (1560 - 1698 m):* Light grey, fine grained rhyolite which is moderately porphyritic with quartz and sanidine phenocrysts. Vein fillings are common while oxidation is mild and pyrite is present in matrix disseminations.

*Trachyte V (1698 - 2130 m) with intrusions:* The trachyte is fine grained, sparsely to moderately porphyritic with sanidine phenocrysts. It is massive to slightly vesicular and shows high alteration intensity of the primary minerals to epidote, prehnite and actinolite. The enhanced alteration is probably the result of several dyke intrusions. Permeability is mainly secondary in the form of veins within the unit.


*Intrusions (2130 - 2690 m):* The lowermost 500 metres of the well consists of intrusives mainly of granitic composition. The intrusives are relatively medium grained, silica rich, with granophyric texture. Occasionally, the alteration minerals epidote, prehnite and actinolite were observed in some units. These intrusive units generally have low permeability.

## 4.2 Hydrothermal alteration

### 4.2.1 Alteration mineralogy of 807A

Several factors, including temperature, rock type, permeability, fluid composition and the duration of the activity affect hydrothermal alteration and mineral formation in geothermal systems. A combination of any of these aspects determine the mineral phases and assemblages that are stable, thus enabling the study of changes with time in a geothermal system (Browne, 1978). The alteration involves the replacement of volcanic glass and primary mineral phases with meta-stable minerals (as shown in Table 2) at prevailing conditions. Generally, hydrothermal alteration in geothermal fields occurs in the temperature range of 150 – 400 °C (Steiner, 1968; Browne, 1978; Browne, 1984a; Browne, 1984b), with resultant textures ranging from partially altered phenocrysts to pervasive alteration of minerals and rock matrix, imparting an earthy aspect to the overall rock (Shanks III, 2012).

TABLE 2: Susceptibility of primary minerals to hydrothermal alteration in Olkaria (modified from Browne, 1984a)

Replacement Order	Primary Minerals	Alteration products
Increasing order 	Volcanic glass	Zeolites, clays, quartz, calcite
	Olivine	Chlorite, actinolite, hematite, clay minerals
	Pyroxene, amphiboles	Chlorite, illite, quartz, pyrite, calcite, actinolite
	Ca- plagioclases	Calcite, albite, adularia, quartz, illite, epidote, sphene
	Sanidine, orthoclase	Adularia
	Fe-Ti oxides	Pyrite, sphene, hematite
	Quartz	No alteration

Common hydrothermal alteration minerals and assemblages in OW-807A characterise the changes in temperature conditions from low to high, indicated by prograde alteration for most of the well sections. Analysis of the alteration mineralogy data, as shown in Figure 7, indicates that the upper zones of the well are mainly characterised by oxidation with commencement of alteration of the volcanic glass in the pyroclastics unit. Within the rhyolites, the alteration of primary minerals is low with alteration being mainly restricted to the glassy fragments and deposition within vesicles and discontinuities. Pyrite is also a common mineral within these zones and is an indicator of the porous character of the lithological units that facilitate circulation of the fluids. This upper zone showing low susceptibility on the replacement of primary minerals generally extends to a depth of approximately 400 m b.g.l.

Below 400 m b.g.l., there is a rapid increase in temperature associated with the circulating geothermal fluids and primary minerals become more susceptible to alteration. Primary ferro-magnesian minerals such as olivine and pyroxenes in basalts are observed to undergo alteration. The ferro-magnesian minerals are observed to alter to clays. Commencement of the alteration of plagioclase and sanidine

feldspars is also observed below this depth, though mainly restricted to the crystal surfaces. Calcite, pyrite, quartz, hematite, sphene and epidote are common replacement minerals. This zone extends to a depth of 600 m b.g.l.

Advanced alteration of the primary minerals is observed below 600 m b.g.l. with the ferromagnesian minerals showing high to pervasive replacement by alteration minerals. Feldspars, mainly forming as phenocrysts, also show moderate to pervasive alteration with depth. Common replacement minerals are calcite, chlorites, illite, epidote, prehnite, wollastonite, adularia, albite, and actinolite. This zone extends to a depth of 2100 m b.g.l.

Below 2100 m b.g.l., the primary minerals are generally slightly altered to secondary minerals, though the sequences present indicate higher temperature in the geothermal system. The limited replacement of these primary phases is associated with the presence of an intrusion. Though the intrusion is associated with higher temperature it is characterised by low permeability, thus causing restriction on the circulation of the hot geothermal fluids. This zone extends to the well bottom. The results of the alteration mineralogy within OW-807A are described in detail in the following sections, based on the analysis from the binocular, polarising microscope, XRD and SEM analysis.

*Zeolites:* XRD analysis of samples from 142-144 m depth shows a peak of 9.0Å with no changes associated with either glycol or heating and is interpreted as mordenite.

*Pyrite:* is common and usually occurs as either surface or rock matrix disseminations or as euhedral crystals in veins and as fracture fillings. In the binocular microscope, it shows a distinctive golden to brassy appearance but appears opaque in the polarising microscope.

*Calcite:* Calcite occurs mainly as a replacement mineral, infilling veins and fractures and rarely as platy calcite. In thin sections, the mineral is characterised by two perfect cleavages, varying relief on rotation in plane polarised light and high interference colours in crossed polars. Twinning is also observed in some of the calcite grains. Calcite extends to 1560 m below the surface, is particularly abundant between 400 and 700 m depth, and is associated with basaltic formations.

*Hematite:* Hematite is a reddish brown to metallic grey oxide in colour which was observed to occur from a relatively shallow depth of 350 m b.g.l. and extending to a depth of 1800 m b.g.l. Hematite in the well forms as either surface disseminations or in euhedral crystals.

*Iddingsite:* Iddingsite is reddish- to brown in colour and mainly associated with the alteration of olivine. Iddingsite forms within the crystal fractures and as distinct rims on the crystals and was observed at a depth of 446 m and 484 m.

*Sphene:* Sphene is a common alteration mineral in the well and was first observed at a depth of 500 m b.g.l., formed as replacement of oxides with increasing temperature. In terms of distribution, sphene is observed to be abundant at depths from 580 m to 650 m b.g.l., 1000 m to 1120 m b.g.l. and 1300 m b.g.l., to 1450 m b.g.l., respectively. In binocular microscope analysis, sphene appears as whitish spots on the mineral surfaces while in thin section it is observed to show high order birefringence colours and high relief.

*Fluorite:* Fluorite is observed as colourless and purple in the binocular microscope, mainly as vesicle and vein filling in well-formed cubes. In thin sections, it is observed as well- formed crystals, either as cubes or octahedral in habit, purple in plane polarized light, and goes into extinction in crossed polars. It is observed sporadically overprinting quartz and quartz-epidote mineral sequences from a depth of 900 m b.g.l. to around 1468 m b.g.l.

*Chalcedony:* Chalcedony mainly shows a first order grey in plane polarised light and goes into extinction in crossed polars. It is observed to occur at depths of 314 m to 416 m b.g.l., commonly deposited in

veins and vesicle fillings and associated with low temperature clays. Chalcedony occurrence is observed in the rhyolites and trachytes forming part of the Upper Olkaria Volcanics lithostratigraphic unit.

*Quartz:* Secondary quartz either forms by the transformation of amorphous silica with increase in temperature, or is precipitated from the supersaturated circulating fluids as crystalline quartz. It is mainly formed in vein fillings and vesicles. Secondary quartz occurrence is consistent from 416 m to 850 m b.g.l., 1100 m to 1400 m b.g.l. and 1550 m to 1850 m b.g.l., respectively, and is a common occurrence in all lithological units in the well. Between depths of 900 m and 1150 m b.g.l. and 1850 and 2650 m b.g.l., quartz is not observed. Quartz is mainly associated with illite and chlorite clays, epidote, prehnite and actinolite mineral assemblages.

*Adularia:* Adularia is observed replacing feldspars in thin sections by its characteristic sectoral extinction in crossed polars beginning at a depth of 1340 m b.g.l. and occurs from there sporadically to the well bottom. Adularia occurrence in the well is observed within rhyolites and trachytes. It is found as abundant vein fillings at a depth of 1340 m b.g.l. with the alteration intensity being moderate to high.

*Albite:* Albite is identified at a depth of 1480 m b.g.l. Albite forms through albitisation of feldspars and the alteration of plagioclases in basalts. In the polarising microscope, it is usually observed as hazy and 'dirty'- strained appearance on the feldspar grains. Albite occurrence in the well is observed to occur within highly altered basalt formations.

*Epidote:* Epidote is first observed at a depth of 532 m b.g.l. and persists to the bottom of the well, often in association with prehnite and predominantly as crystalline and vein fillings. In thin sections, epidote forms prismatic crystals, pleochroic in hues of yellow to green with high relief in plane polarised light and high birefringence colours in crossed polars. Observations made through the binocular microscope show a colour gradation from the characteristic yellowish-green to a more greenish colouration at a depth of 1400 m. Epidote is observed in abundance from 532 m to 650 m b.g.l., 800 m to 900 m b.g.l., and 1200 m to 1850 m b.g.l., respectively, while it is also sporadically observed at other depths, associated with rhyolites, basalts and trachytes units.

*Prehnite:* Prehnite, first observed at 646 m b.g.l., occurs mainly in association with epidote, either as alteration of feldspars or as precipitation in veins and vesicles from 600 m to 2040 m b.g.l. and sporadically down to 2400 m. In plane polarised light, it is colourless, characterised by high relief, in prismatic crystals, and shows high birefringence colours in crossed polars.

*Wollastonite:* Wollastonite is first observed at a depth of 720 m b.g.l. and forms either by replacement of calcite or by high temperature alteration of pyroxenes. In thin sections, it is pale brown to colourless, forming clusters of radiating fibres and shows a low birefringence yellow to orange colour of the first order in crossed polars. Between 720 m and 1300 m b.g.l., wollastonite occurs sporadically while it is relatively abundant at depths from 1300 m to 1600 m b.g.l. and is mainly associated with the trachytes and basalts.

*Actinolite:* Actinolite's first appearance was at a depth of 664 m and it forms as a replacement of clinopyroxenes and precipitates in vesicles. Occurrence of actinolite is observed to occur between the depths of 664 m and 810 m b.g.l. and between 1278 m and 2200 m b.g.l. Between 810 m and 1278 m b.g.l., actinolite is not observed in the alteration mineral assemblages. Actinolite is observed to form ordered fibrous aggregates, usually pleochroic in hues of green, with a high relief in plane polarised light and high birefringence colours in crossed polars and is commonly found in basalts, trachytes and the rhyolites in the well. Figure 8 shows the alteration minerals as observed in the polarising microscope.

**KENGEN:**

**Well Data:**

Field Name: **Olkaria South East**

Location: **South East**

Well Name: **OW 807A**

**Site Data:**

Eastings: **200,613.761 m**

Northings: **9,899,580.653 m**

Elevation: **1,898.24 m**

**Drilling Data:**

Depth Range: **0-2690 m**

Production Casing: **1004 m**

Drilling Rig: **N370 /Kgn 2**

Geologist: **Danson Warui**

Spud date: **13.06.2017**

Completion date: **24.04.2018**

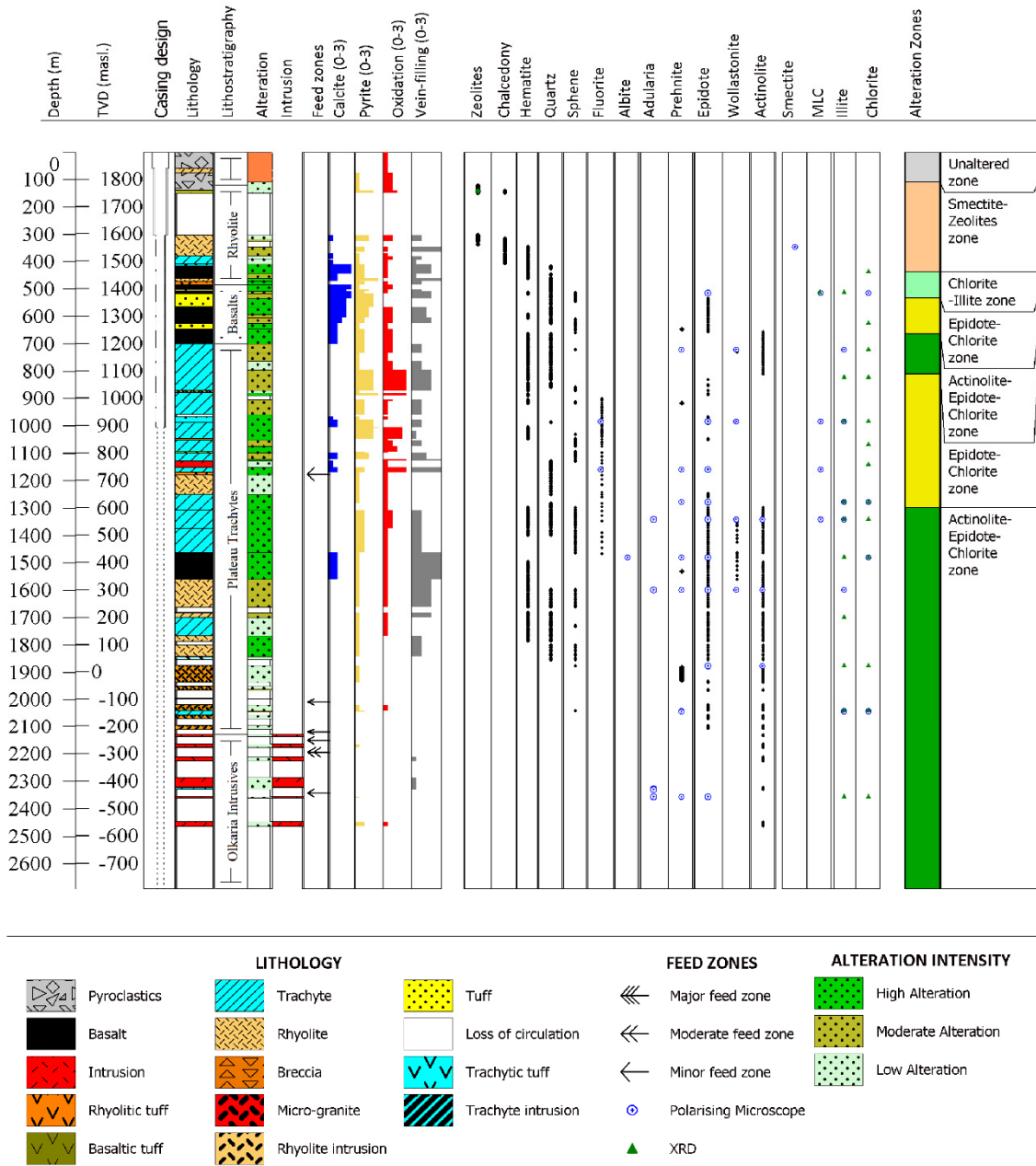


FIGURE 7: Lithology and alteration mineralogy of well OW-807A

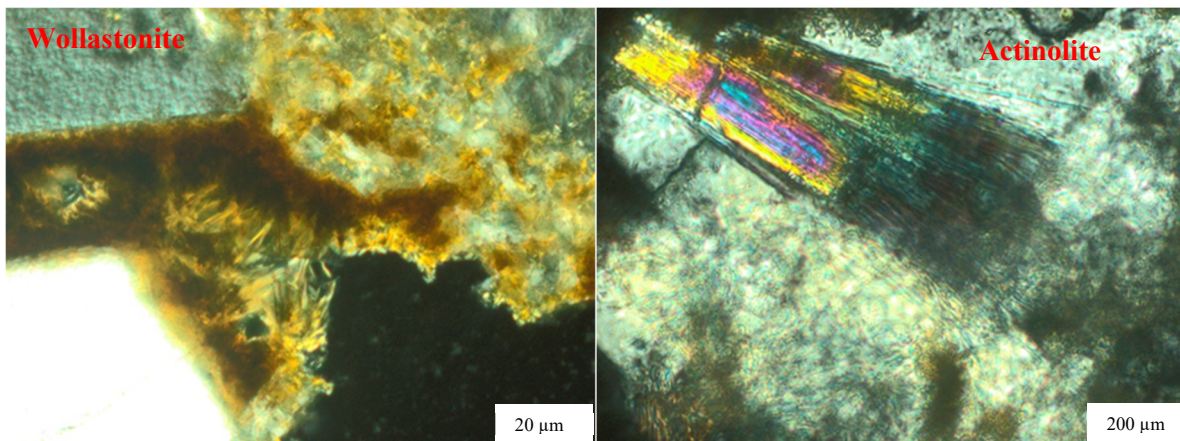


FIGURE 8: Wollastonite (720-722 m) and actinolite (1598-1600 m) observed in well OW 807A

#### 4.2.2 Alteration mineral paragenesis and zonation

Alteration minerals and mineral sequences detail the variability of the physical and chemical conditions in an active geothermal system, including temperature, fluid composition, permeability and rock fluid interactions. The analysis of the minerals and sequences provides a fair indication of conditions and variations that have occurred through time, thus playing a key role in the reconstruction of the history of a geothermal system. Alteration mineral paragenesis and zonation in OW-807A can be generally categorised into sequences that show variations in temperature conditions and sequences that relate to the permeability conditions within the well (Figure 7). A summary of these mineral sequences as observed during analysis of well rock cuttings and thin sections is tabulated in Table 3.

In terms of thermal changes, the flowing sequences are considered representative of the changes that have occurred within the system over time. Within the shallow depths of the well, precipitation of zeolites, chalcedony, clays and quartz mineral sequences indicates the increase of temperature with depth, from temperatures of 50°C to temperatures of >180°C. Sequences in vein-fillings and vesicles characterised by quartz >> epidote, clays >> calcite >> epidote, and quartz >> actinolite, show that the temperatures have increased to 280°C. An exception from this normal progradation of alteration facies is when lower temperature minerals imprint over the higher temperature minerals, indicating a possible temperature reversal. The formation of clays >> epidote >> calcite as vein filling as observed at a depth of 966 m indicates a possible lowering of the circulating geothermal fluid's temperatures. At a depth of between 900 m and 1468 metres, fluorite is observed imprinting existing mineral sequences including quartz and epidote.

Alteration minerals considered to represent the permeability conditions intersected by the well include pyrite, calcite and adularia. The occurrence of pyrite >> clays at a depth of 508 m b.g.l. is thought to represent conditions of decreasing permeability as the formation of clays fills up the voids. The sequence quartz >> clays >> adularia at 1340 m b.g.l. represents highly permeable conditions. Though the formation of clays may have initially been associated with reduced porosity, it is considered likely that events after the clay deposition have caused the re-opening of these veins. These re-opened veins then indicate enhanced permeability allowing the adularia to be deposited. Also, the occurrence of quartz >> albite sequence indicates the presence of highly permeable conditions. This conclusion is based on the fact that the formation of albite and adularia requires the mobilisation of ions and permeable conditions are needed to facilitate their movement to the reaction sites.



TABLE 3: Mineral sequences observed in well OW-807A

Depth (m)	Mineral sequences											Type	Remarks	
	Z	Cy	Cla	F	Q	Ch	Ca	Py	Pn	E	A			Ad
374-376 390-392	2	1	3										v, v-f	Mineral sequences characteristic of increase in temperature with depth, a result of elevated geothermal gradient
416-426			1		2								v-f	
			1				2							
508-516			2					1					v-f	
			1				2							
604-606					1					2			v-f	
720-722			1		2								v-f	
966-968			1				3			2			v	Reversals in temperature within this zone
982-986			1	2	3								v	
			1		2								v-f	
1158-1162					1					2			v-f	
			1	2										
1166-1168					1	2							v	
1340-1344			1		2							3	v	Prograde mineral sequences, indicating recovery and temperature increase with depth
1384-1386					1						2		v	
1448-1450					1	2							v-f	
1464-1468					3	1				2			v	
1480-1484					1					3	2		v-f	
					1						2			
1598-1600					1					3	2		v-f	
1994-1996					1					2			v-f	
<b>Key</b>				Cy- Chalcedony		Cla- clays		Fl- Fluorite		Q- quartz		Ch- chlorite		
V-f- vein filling,				Ca- calcite		Py- Pyrite		Pn- prehnite		E-epidote		A-actinolite		
V- vesicle				Ad- adularia		Z- zeolite								
<b>1, 2, 3 - Order of placement, oldest (1) to youngest (3) in vesicles and vein-fillings</b>														

The alteration zonation for well OW-807A is based on the first appearance of key index minerals that are considered stable at specific temperature ranges. These include zeolites, smectite clays, quartz, chlorite, epidote and actinolite, representing temperatures of below 150°C (zeolites) to above 280°C (actinolite) in the geothermal system. These zones have been categorised into unaltered zone, smectite-zeolites zone, chlorite-illite zone, epidote-chlorite zone and actinolite-epidote-chlorite zone and are described in detail in the following section.

*Unaltered zone (0-110 m):* This zone extends from the surface to a depth of 100 m b.g.l. and is characterised by the absence of hydrothermal alteration with the rocks being relatively fresh and massive. However, oxidation is common and is attributed to the interaction between the rocks and the percolating meteoric fluids from the surface. This zone is above the current groundwater level, which is slightly below 400 m b.g.l.

*Zeolites-smectite zone (110-436 m):* This zone is characterised by zeolites and smectite clays, representing temperatures of 50°C to < 200°C. In this zone, alteration of primary minerals is relatively low, mainly restricted to the groundmass and as depositions within fractures and vesicles, with the phenocrysts largely remaining unaltered. Through XRD analysis, the zeolites were identified to be mordenite which are commonly associated with highly evolved rhyolites. Common mineral assemblages within this zone are smectite clays, zeolites, chalcedony, pyrite and minor calcite. The zeolites were first observed at a depth of 140 m b.g.l.

*Chlorite-illite zone (436-532 m):* This zone is characterised by the occurrence of chlorites and illite clays representing temperatures of  $> 200^{\circ}\text{C}$ . Chlorite clays are mainly associated with the alteration of mafic minerals in the host rock as a result of hydrothermal processes. In this zone, pyroxenes and augite show enhanced alteration to chlorites in comparison to the felsic minerals which show moderate alteration intensity. The clays form as matrix clays and as depositions in vesicles, fractures and vein fillings. In addition to chlorites and illite, other common mineral assemblages in this zone are quartz, calcite and pyrite.

*Epidote-chlorite zone I (532-664 m):* This zone is marked by the first appearance of epidote at a depth of 532 m b.g.l., indicating temperatures of above  $240^{\circ}\text{C}$  in the geothermal system. Within this zone, primary minerals have been subjected to enhanced alteration, signifying the increasing thermal regime of the circulating hydrothermal fluids resulting in increased water-rock interactions. Alteration mineral assemblages in this zone include epidote, prehnite, quartz, chlorite, pyrite, calcite and sphene. Calcite is mainly replacement calcite and is closely associated to the basaltic units. Vein fillings and pyrite are abundant in this zone, indicating the highly permeable conditions.

*Actinolite-epidote-chlorite zone I (664- 810 m):* This zone is marked by the first appearance of actinolite at a depth of 664 m to 810 m b.g.l., representing temperatures above  $280^{\circ}\text{C}$ . Common mineral assemblages include actinolite, epidote, prehnite, wollastonite, illite, chlorite, quartz and sphene.

*Epidote-chlorite zone II (810-1298 m):* This zone shows similar characteristics as the Epidote- Chlorite Zone I described above. Common alteration mineral assemblages include epidote, prehnite, wollastonite, quartz, chlorite, illite, sphene and hematite. The abundance of pyrite, vein fillings and oxidation indicate high permeability in this zone. Secondary fluorite deposition is also observed.

*Actinolite-epidote-chlorite zone II (1298- 2690 m):* The zone is characterised by the re-appearance of actinolite at a depth of 1298 m b.g.l. extending to the well bottom. Mineral assemblages within this zone consist of actinolite, epidote, prehnite, albite, adularia, wollastonite, illite and chlorite clays.

### 4.3 Well OW-807A hydrothermal clay analysis

The importance of clay minerals in active geothermal systems is key in the determination of the main factors controlling alteration mineral assemblages. Different workers including Steiner (1968), whose work forms the earliest attempts to link temperature to clay minerals, realized the important role played by clay minerals in addition to other silicate minerals as described in Browne (1970). The formation of different types of hydrothermal clays in active geothermal systems offers insight into the variability of the conditions with temperature playing a major role together with composition, solution pH and fluid rock ratio. Within these systems, the alteration of primary minerals and direct precipitation processes may occur, either simultaneously or successively, depending on the location and duration of the activity and if rapid changes occur over time, several clay formation episodes may be recorded in the same rock resulting in a complicated combination of different clay species (Meunier, 2005). Thus, the systematic studies carried out on clay assemblages on their occurrence, composition and paragenesis can be utilised to reconstruct the thermal evolution of a geothermal system, with illite and chlorite being the most common (Battaglia, 2004; Cathelineau, 1988).

A plot comparing the weight percentages of MgO and FeO in samples from different depths shows that there are some variations (Figure 9). The semi-quantitative analysis for both illite and chlorite shows three possible groupings, one group is characterised by a high MgO content and low FeO, another by moderate MgO and FeO, and a third is characterised by low MgO and very high FeO content. The clays at 1480 m b.g.l. are relatively enriched in magnesium. Compositional element maps in Appendices 1 and 2 show the variations of the different elements for the clays. Generally, there is an overall reduction in the Fe content with depth.

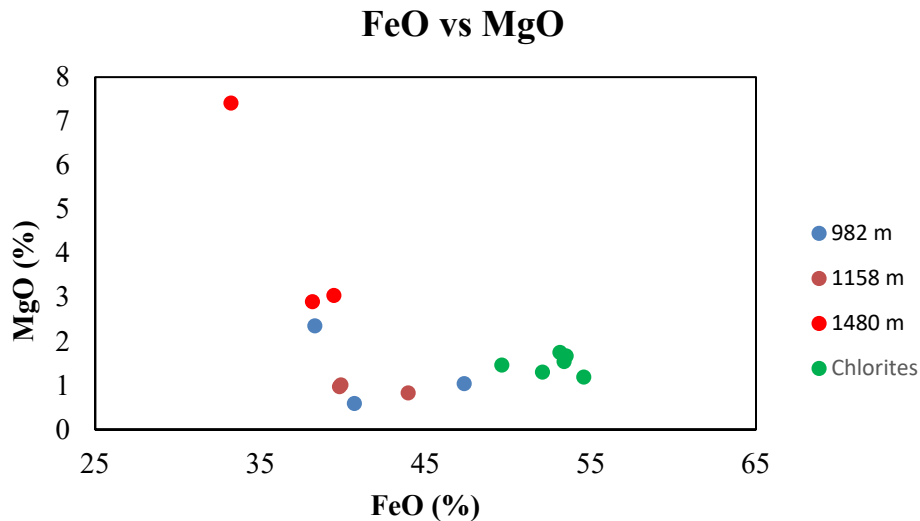


FIGURE 9: FeO vs MgO weight percent for the illite and chlorite clays in well OW-807A

#### 4.3.1 Smectites

In OW-807A, smectite clays were observed at a depth of 342 m b.g.l. In the polarising microscope, smectites are identified being brown to pale green, very fine grained in plane polarised light, formed from the alteration of volcanic glass and infilling vesicles. The occurrence of smectite clays in the well is restricted to the upper sections of the well and they are considered to have formed at depths shallower than 342 m b.g.l. Note that and the indicated depth only shows where the samples were available for thin section analysis.

#### 4.3.2 Mixed Layer clays

Mixed layer clays represent intermediate products of reactions involving pure end member clays and essentially involve two components, with varieties such as chlorite/smectites and Illite/ smectites being common in hydrothermal alteration paragenesis.

In OW-807A, mixed layer clays were first observed at a depth of 512 m, based on XRD analysis. In the polarising microscope, they are weakly pleochroic from pale yellow to brown in plane polarised light, with high order birefringence colours in crossed polars and are observed to occur to a depth of 1300 m b.g.l.

Analysis of the diffractograms from XRD analysis shows distinct peaks at  $d(001)$ , with ethyl-glycol at  $31.1\text{ \AA}$  and another at  $15.9\text{ \AA}$ , air-dried at  $14.3\text{ \AA}$ , and the heated peak is plateauing for both  $d(001)$  and at  $7.1\text{ \AA}$ ,  $d(002)$ . The ethylene glycol peak shows the existence of a swelling component, probably of smectite composition, while the latter peak shows the presence of a chlorite layer within the clay mineral. The analysis is interpreted to be indicative of corrensite (Lagat, 2010) and the diffractogram is shown in Figure 10.

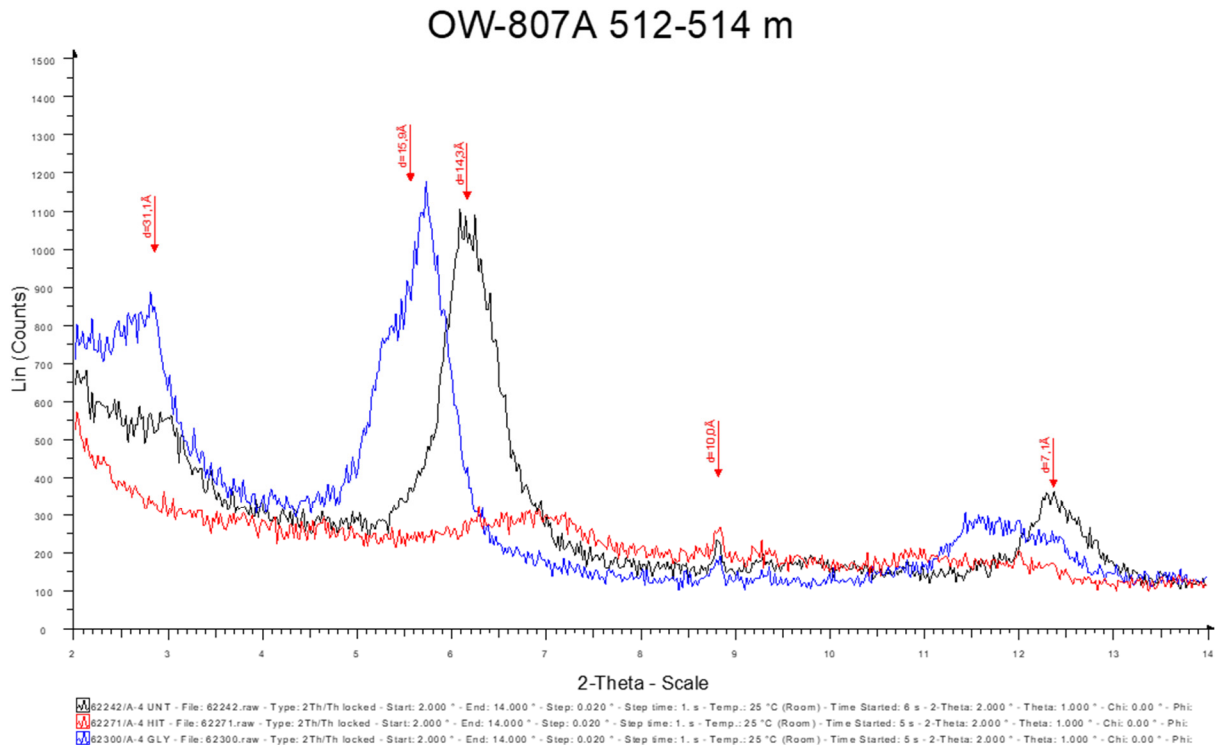


FIGURE 10: Diffraction pattern for mixed layer chlorite/smectite at 512-514 m in well OW-807A

### 4.3.3 Illite clays

Illite was first observed at a depth of 512 m, based on XRD analysis, as traces within the basalt IV unit. In thin sections, illite is observed forming flakes that show an intense white to speckled appearance in crossed polars and it forms through the alteration of primary minerals and as depositions in fractures. Illite is the product of alteration of sanidine feldspars in more evolved lithology units, in this case within the trachytes and rhyolites. However, it also forms in basalts, attributed to the presence of K-rich fluids circulating in a reservoir.

In XRD analysis diffractograms, it is characterised by distinct  $d(001)$  peaks of 9.93 Å to 10.2 Å, for air-dried samples, with no changes in the ethyl-glycol and 550°C heated samples as shown in Appendix 3. Studies have shown that the slight shifting of the peaks is attributed to the K- saturation and trapped fluids in the crystal structure (Hower and Mowatt, 1966).

In the SEM analysis, the illite appears as both fibrous and as flakes forming from alteration of feldspar. The fibrous or 'hairy' like morphology as shown in Figure 11 is attributed to minor substitutions in the octahedral of K by Na, Mg and Ca (Deer et al., 1992). The structural determinations of the compositional data based on 24 oxygens as obtained from the microprobe analysis is shown in Table 4. The chemical composition data shows high Fe enrichment with minor contents of Na and Mg.

TABLE 4: Illite clay compositional data for well OW-807A

Analyses	1	2	3	4	5	6	7	8	9
Depth	982m	982m	982m	1158m	1158m	1158m	1480m	1480m	1480m
SiO <sub>2</sub>	45.14	36.85	46.17	44.43	48.15	48.01	48.65	39.32	47.97
TiO <sub>2</sub>								0.71	
Al <sub>2</sub> O <sub>3</sub>	10.01	11.55	7.01	4.83	5.46	5.32	5.40	9.78	4.75
Fe <sub>2</sub> O <sub>3</sub>									
FeO	38.31	47.35	40.70	43.95	39.89	39.80	38.16	33.23	39.46
MgO	2.35	1.04	0.59	0.83	1.01	0.97	2.90	7.41	3.04
CaO		0.37							
Na <sub>2</sub> O			0.85	0.63	0.92	0.77	0.98		0.70
MnO	2.26	1.61	2.45	2.37	2.00	2.06	1.87		1.99
K <sub>2</sub> O	1.92	1.23	2.24	2.64	2.58	2.54	2.04	9.55	3.08
<b>Total</b>	<b>99.99</b>	<b>100.00</b>	<b>100.01</b>	<b>99.68</b>	<b>100.01</b>	<b>99.47</b>	<b>100.00</b>	<b>100.00</b>	<b>100.99</b>
<b>Numbers of ions (24 Oxygen Basis)</b>									
Si	7.387	6.417	7.696	7.633	7.967	7.987	7.946	6.700	7.875
Al	0.613	1.583	0.304	0.367	0.033	0.013	0.054	1.300	0.125
Al	1.318	0.788	1.073	0.611	1.032	1.030	0.986	0.663	0.794
Ti	0.000	0.000	0.000	0.000	0.000	0.000	0.000	0.000	0.000
Fe <sup>3+</sup>									
Fe <sup>2+</sup>	3.495	4.597	3.782	4.210	3.680	3.691	3.475	3.157	3.612
Mg	0.573	0.270	0.147	0.213	0.249	0.241	0.706	1.882	0.744
Ca	0.000	0.069	0.000	0.000	0.000	0.000	0.000	0.000	0.000
Na	0.000	0.000	0.275	0.210	0.295	0.248	0.310	0.000	0.223
Mn	0.313	0.237	0.346	0.345	0.280	0.290	0.261	0.000	0.277
K	0.401	0.273	0.476	0.579	0.545	0.539	0.425	2.076	0.645

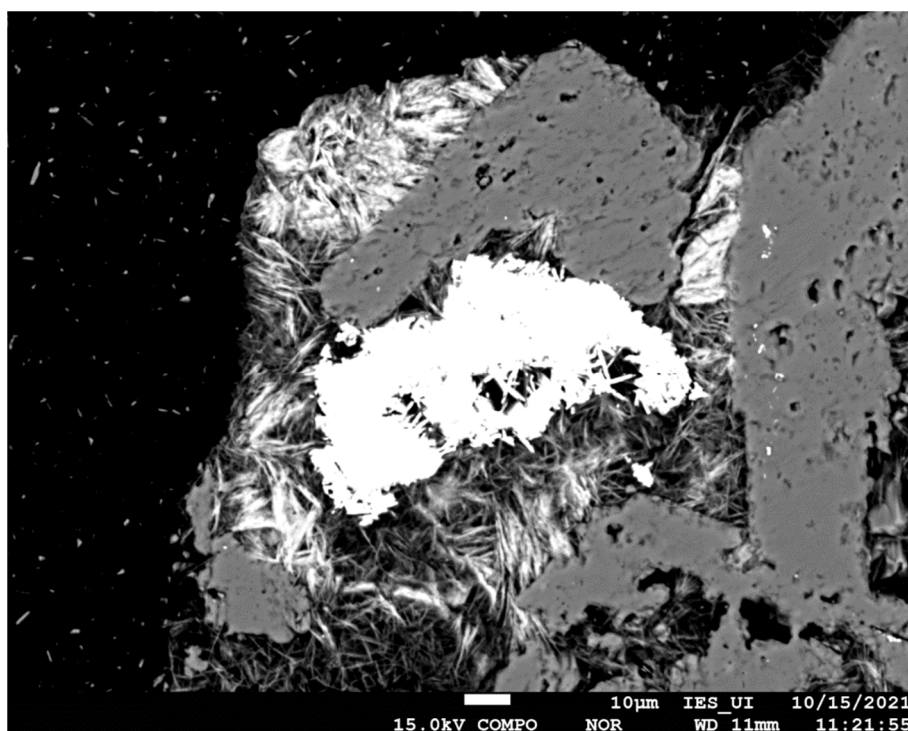


FIGURE 11: SEM image of fibrous illite at 1158 m b.g.l. in well OW-807A

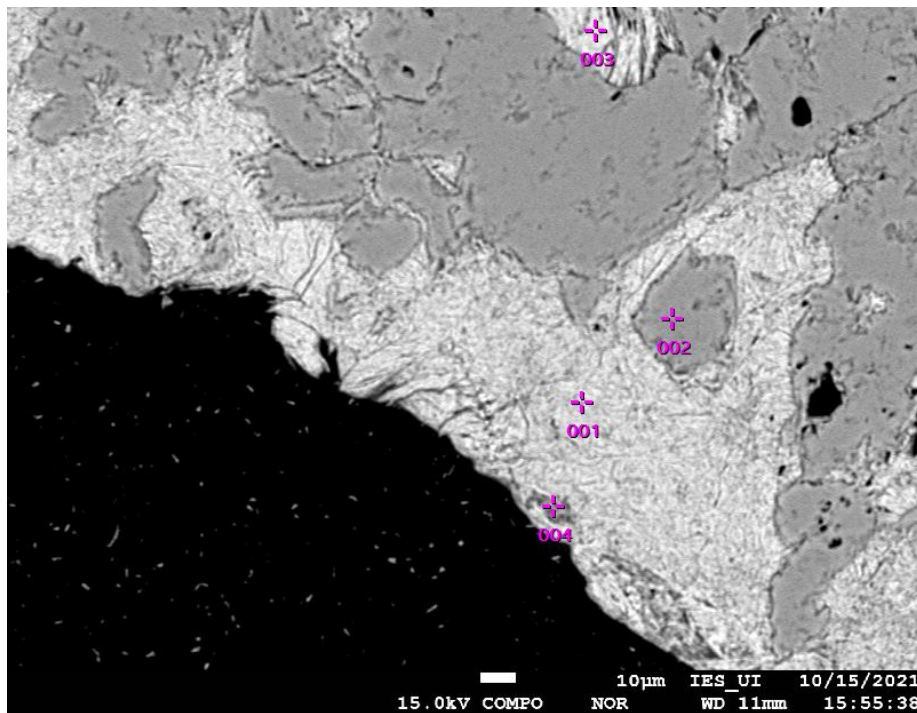


FIGURE 12: Illite clays from the alteration of feldspar at 1480 m b.g.l. in well OW-807A

The compositional data in Figure 11 is shown in Table 4 columns 4, 5 and 6, while the illite compositional data at 1480 m depth in Figure 12 is shown in columns 7, 8 and 9, with the elemental composition maps shown in Appendix 1 of the report.

#### 4.3.4 Chlorite clays

The chlorite structure consists of alternating layers of brucite-like and negatively charged mica-like layers due to replacement of Si by Al in the four-fold position. This is balanced by a corresponding number of Al atoms replacing divalent ions in the six-fold position in the brucite-like layer, thus allowing extensive substitution with no apparent miscibility gaps. Small amounts of Mn, Ti, Cr, Ca, Na, and K have been reported, where Mn and small amounts of Ca are thought to substitute directly for Fe and Mg, while Ti may be due to fine inclusions of ilmenite, rutile or titanite in the six-fold position and the replacement of OH by F and Cl (Albee, 1962).

Chlorite was first observed in OW-807A at 436 m depth based on XRD analyses of the basaltic lithological unit. Chlorite mainly forms from alteration of ferromagnesian minerals and is usually associated with other high temperature mineral assemblages such as epidote, actinolite, or wollastonite, indicating propylitic hydrothermal alteration facies. In thin sections, chlorite shows pleochroism in green under plane polarized light with no changes in crossed polars and exhibits low birefringence colours of blue and yellow of the first order.

The analysis of diffraction patterns for chlorites shows a distinct peak of 14.2 Å, d (001), for air-dried, ethyl-glycol, and heated samples at 550°C, as shown in Appendix 3. Within the Olkaria Geothermal Field, there occurs a more prominent second order peak at 7.1Å, which is characterised by the disappearance of the heated peak and has been described as a form of unstable chlorite (Moore and Reynolds, 1997).

The XRD patterns also show the existence of another clay with a distinct d (001) spacing of between 12.3 Å to 12.4 Å, which shows no change with glycolation. A slight change when heated to 550°C may

represent randomly interstratified chlorite-illite. This is also indicated by the SEM analysis where chlorite and illite were observed interstratified (Figure 13) at a depth of 982 m b.g.l.

SEM analysis of the clays, as shown in Figure 12 and 13, shows the existence of textural variations in the chlorite clays, ranging from the relatively coarse grained to the relatively fine-grained variety. Compositional analysis shows that the chlorites are relatively enriched in Fe, with a ternary plot obtained from the comparison of the Al vacancy in the tetrahedral, Mg and Fe (Figure 15) indicating that they plot within the range occupied by chamosite. Compositional data for the chlorite analysis based on 36 oxygens is tabulated in Table 5 with the corresponding structural data for the tetrahedral and octahedral site occupancy, while the elemental composition maps of the chlorite clays is as shown in Appendix 2.

TABLE 5: Compositional data for the analysed chlorite clays for well OW-807A

Analysis/ column	1	2	3	4	5	6
Depth	982 m	982 m	982 m	982 m	982 m	982 m
SiO <sub>2</sub>	26.65	28.10	26.05	28.34	28.62	28.79
TiO <sub>2</sub>						
Al <sub>2</sub> O <sub>3</sub>	16.72	14.78	14.30	16.54	15.25	16.28
Fe <sub>2</sub> O <sub>3</sub>						
FeO	53.52	53.14	49.62	52.08	54.58	53.39
MgO	1.67	1.75	1.46	1.30	1.19	1.54
CaO						
Na <sub>2</sub> O						
MnO	1.44	1.47	1.23	1.38		
K <sub>2</sub> O				0.36	0.36	
<b>Total</b>	<b>100.00</b>	<b>99.24</b>	<b>92.66</b>	<b>100.00</b>	<b>100.00</b>	<b>100.00</b>
<b>Numbers of ions (36 Oxygen Basis)</b>						
Si	7.305	7.744	7.681	7.682	7.814	7.775
Al	0.695	0.256	0.319	0.318	0.186	0.225
Al	4.707	4.545	4.650	4.966	4.722	4.957
Ti	0.000	0.000	0.000	0.000	0.000	0.000
Fe <sup>3+</sup>						
Fe <sup>2+</sup>	8.180	8.165	8.157	7.871	8.309	8.039
Mg	0.682	0.719	0.642	0.525	0.484	0.620
Ca	0.000	0.000	0.000	0.000	0.000	0.000
Na	0.000	0.000	0.000	0.000	0.000	0.000
Mn	0.334	0.343	0.307	0.317	0.000	0.000
K	0.000	0.000	0.000	0.124	0.125	0.000

The compositional data for the data points shown in Figure 13 is captured in Table 5, columns 1 and 2. Analysis points 1 and 2, as shown in Figure 14, are shown in Table 5, columns 4 and 5 while points 3 and 4 are shown in Table 4 columns 1 and 2.

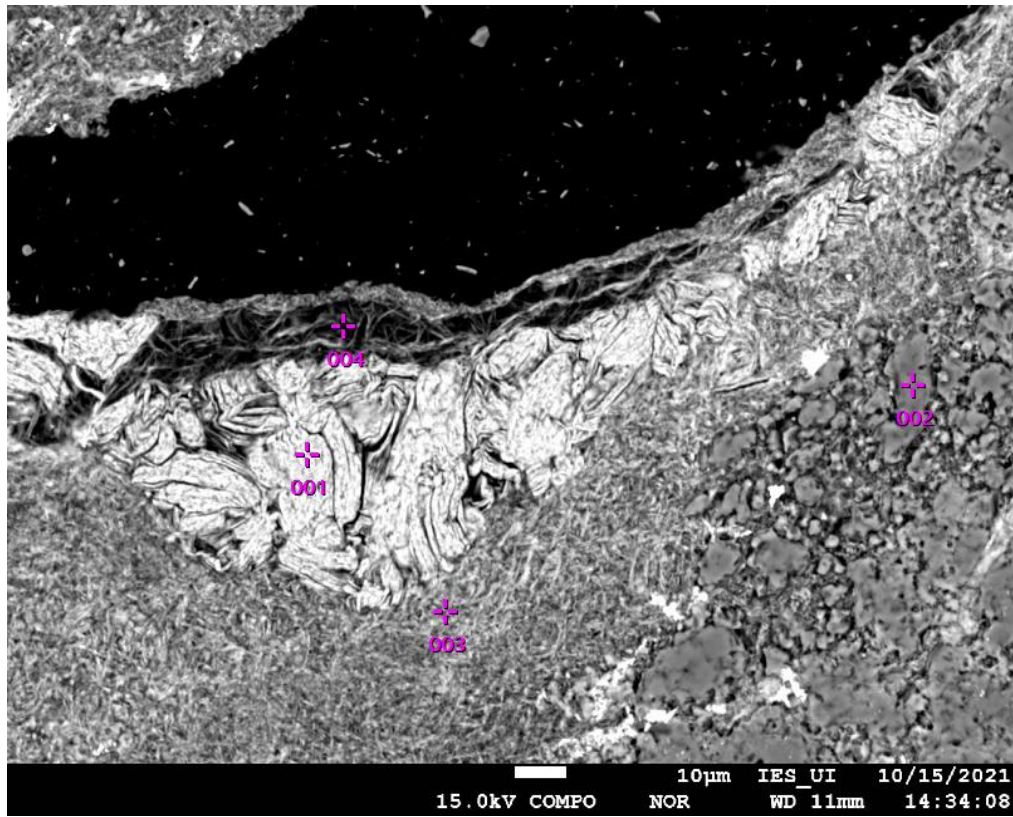


FIGURE 13: Chlorite clays showing variations in the texture at 982 m b.g.l. in well OW-807A

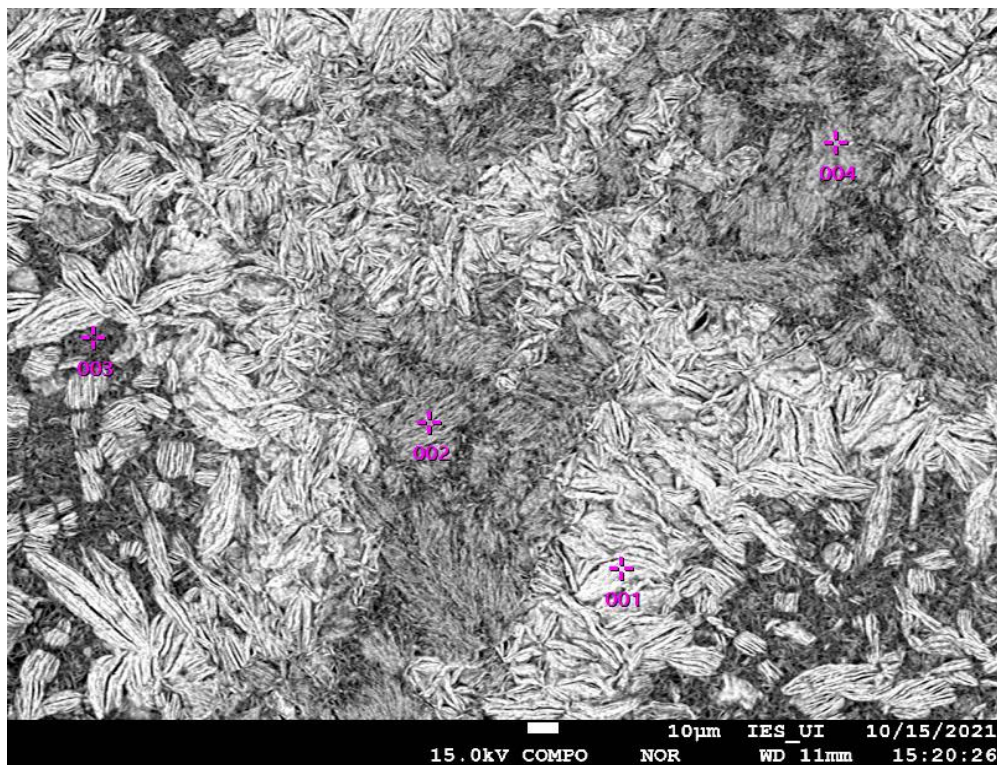


FIGURE 14: Chlorite and Illite clays intergrowth at a depth of 982 m b.g.l. in well OW-807A



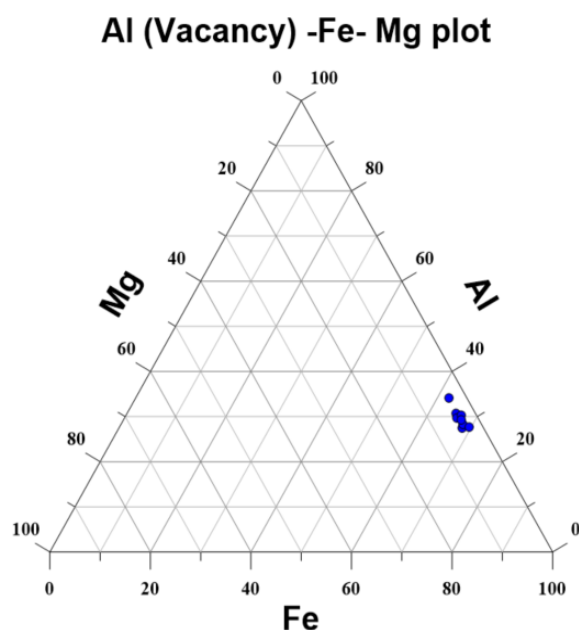


FIGURE 15: Al (IV) vs Fe vs Mg ternary plot for well OW-807A

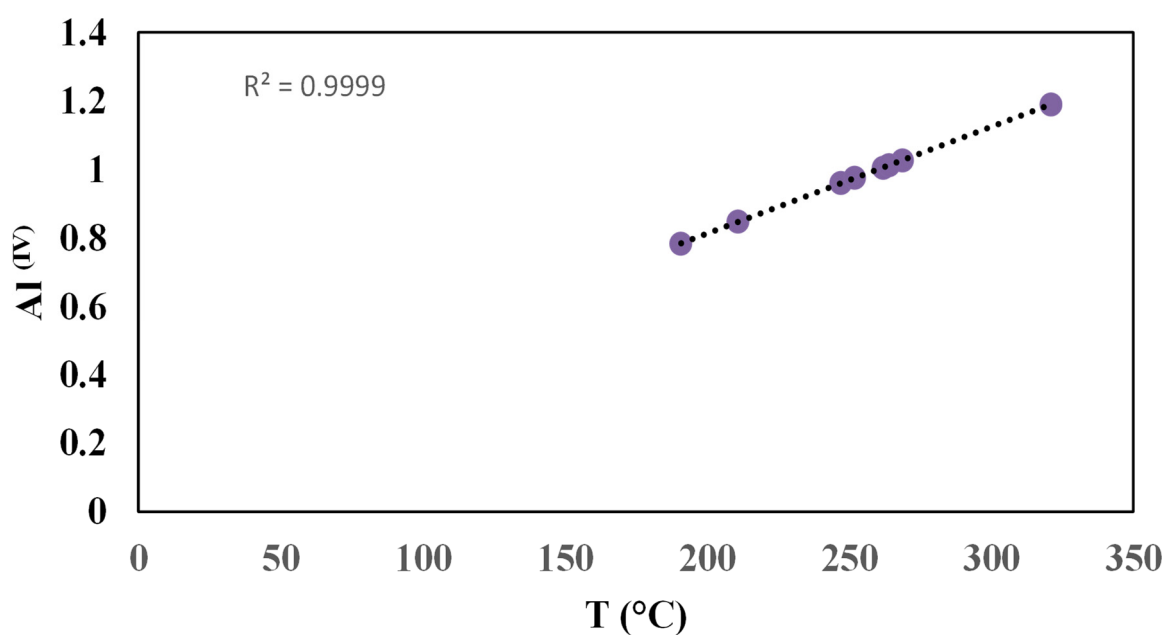


FIGURE 16: Al (IV) vs Temperature plot for chlorites in OW-807A

Temperature calculations for chlorite at a depth of 982 m b.g.l. based on the tetrahedral vacancy of Al, a method proposed by Hillier and Velde (1991), were carried out, using the WinCcac program (Yavuz et al., 2015) based on 28 oxygens. The temperatures show a range between 191°C and 321°C (Figure 16).

A summary of the clay types based on XRD analysis is tabulated in Table 6.

TABLE 6: Summary of XRD clay analysis for well OW-807A

Depth (m)	d (001)			d (002)			Rock type	Remarks
	A	E G	H	A	E G	H		
142-144	9.0	9.0	9.0				Rhyolitic tuff	Mordenite
	10.1	10.1	10.1					Illite traces
	8.5	8.5	8.5					Amphiboles
346-350	-	-	-	7.2	7.2	-	Rhyolite	Kaolinite?
	-	-	-	6.5				Feldspars
512-514	31.1	14.3	-	7.1	7.1	-	Basalt	Chlo: Sm
	10	10	10					Illite traces
624-626	14.5	14.5	14.5	7.1	7.1	7.5	Basalt	Chlorite
720-722	12.4	12.4	12.4	7.2	7.2	-	Rhyolite	Chlorite
822-824	12.4	12.4	12.4	7.2	7.2	-	Trachyte	Chlorite
	10.2	10.2	10.2					Illite
982-986	12.4	12.4	12.4	7.2	7.2	-		Chlorite
	10.1	10.1	10.1					Illite traces
1158-1162	12.1	12.1	12.1	7.1	7.1	-		Chlorite
1278-1280	12.3	12.3	12.3	7.1	7.1	-	Trachyte	Chlorite traces
	10.1	10.1	10.1					Illite traces
1340-1344	12.1	12.1	12.1	7.1	7.1	-	Trachyte	Chlorite traces
	10.07	10.07	10.07					Illite
1480-1484	14.25	14.25	14.25	7.13	7.13		Basalt	Chlorite
	10.10	10.10	10.10					Illite
1876-1880	9.93	9.93	9.93				Micro-granite	Illite
2040-2044	12.26	12.26	12.26	7.1	7.1		Rhyolite	Chlorite
	10.1	10.1	10.1					Illite traces
2356-2360	12.26	12.26	12.26	7.1	7.1		Micro-granite	Chlorite traces
	10.1	10.1	10.1					Illite traces

A: Air-dried E G: Ethyl-glycolated H: Heated (550°C)

#### 4.4 Permeability controls on the alteration mineralogy of OW-807A

The permeability in the greater Olkaria Geothermal field is mainly associated with faults and fractures, while horizontally it is predominantly related to contacts between lava flows and tuff horizons. Aquifers in Olkaria produce at temperatures between 190 and 270°C and within this range, close to sixteen mineral types have been identified including adularia, albite, biotite, calcite, chlorite, epidote, Fe-oxides, fluorite, garnet, illite, prehnite, pyrite, quartz, smectite, and wairakite. Assuming that minerals are stable over a given temperature-pressure range, the phase rule does not allow such high numbers of minerals as major components, as they should be approximately ten. It is thus imperative that the presence of some of the minerals must be a consequence of variable rock composition, changes in temperature with time, or the extent of water rock interactions (Karingithi et al., 2010). This emphasises the importance of permeability in the facilitation of water-rock interactions in this field.

According to Munyiri (2016), fractures form the main avenue of bulk fluid transport, especially where they form systems of interconnected clusters, with the associated permeability being dependent on regional and local fracture trends. Characterisation of these fractures in the current study involved the identification of fractures, veins and vein fillings from the well drill cuttings and rating their relative quantity on a scale from 1 to 3, with 3 being the highest number observed in a sample.

The permeability of OW-807A, as deduced from the alteration mineralogy, indicates a permeable system to depths of approximately 2000 metres below ground level, below which the permeability is highly reduced, attributed to the granitic intrusion at that depth. Below this depth, permeability is mainly

associated with the intrusive contacts where their emplacement has caused localised stress on the host reservoir rock. Generally, a comparative analysis between the different depths based on mineral assemblages shows that the relatively permeable zones have an assortment of different minerals. Based on this, the well has been categorised into three zones, i.e., Zone I between 400 m and 1200 m b.g.l., Zone II between 1300 m and 1900 m b.g.l. and Zone III below 2100 m b.g.l., respectively.

Zone I is relatively permeable with temperatures of  $>180^{\circ}\text{C}$ , based on the alteration minerals. This zone is characterised by a wide range of alteration minerals, including calcite, oxides, pyrite, sphene, quartz, prehnite, epidote, wollastonite, actinolite and the hydrothermal clays. Zone II is also relatively permeable with the occurrence of adularia and albite in this depth range. Hydrothermal alteration involves reactions between the different phases leading to the formation of secondary metastable minerals. The albitisation process and the conversion of feldspars to adularia requires a highly permeable system that easily mobilises the reactants to suitable reaction sites. The deposition of these minerals is thus deduced to be the result of enhanced permeability within the 400 m b.g.l. to 1200 m b.g.l. depth range. Zone III mainly covers the depths characterised by the intrusives and shows a reduced alteration intensity. Alteration mineral assemblages include actinolite, prehnite- epidote, and hydrothermal clays. Permeability is mainly restricted to contact zones between the intrusion and the host country rock. The alteration rank indicates that this zone was characterised by paleo-temperatures of  $>240^{\circ}\text{C}$  although current conditions indicate lower temperatures.

The smectite-to-chlorite transition in mixed layer clays relates to an increase of the formation temperatures from  $160\text{-}180^{\circ}\text{C}$  to  $240\text{-}250^{\circ}\text{C}$  while the smectite-to-illite transition indicates temperatures of  $150\text{-}220^{\circ}\text{C}$  (Fulignati, 2020). The transformation of smectite to chlorite, is characterised by the decrease in the percentage of smectite layers in the interstratified chlorite/smectite, with increase in temperature, with notable steps at 100-80%, 50-40% and 10-0%. The 50-40% step is characterised by the formation of corrensite at the 50-40% step, a thermodynamically stable phase of the transformation, with temperatures of  $100\text{-}200^{\circ}\text{C}$  and permeable zones favouring its formation (Inoue and Utada, 1991). The wide difference in observed temperatures for the transformation is generally attributed to permeability. Highly permeable systems support a dissolution-precipitation mechanism enabling chlorite to precipitate directly from the fluids, whereas in low permeability systems, where fluid movement is restricted to pores, gradual transformation of smectite to illite occurs and chlorite thus forms as a by-product of this transformations (Harvey and Browne, 1991).

The textural variations in the clays may be inferred to be representative of the prevailing permeability conditions during their emplacement. The occurrence of chlorites in varying textures, varying between fine and coarse grained, may be a result of a change in permeability. The precipitation of the illite in the fibrous or 'hairy' morphology may be related to the presence of a highly porous medium allowing for their unhindered deposition.

A comparison between the alteration temperatures indicates that in the past temperatures were higher than they are at present. The temperature plots in Figure 17 show that there exists a shallow high temperature influence on the alteration mineralogy. The upper section of the well, 400 m – 700 m b.g.l., shows a rapid increase in temperature, facilitating the occurrence of epidote and actinolite at relatively shallow depths of 532 m and 664 m b.g.l. This is interpreted to represent the proximity of the well to an up-flow zone in this part of the field. However, as the well is deviated, it gradually moves away from this up-flow zone and the bottom sections are interpreted to intersect a deep convective geothermal system. Towards the deeper sections, the well encounters dykes and a massive granitic intrusion at 2130 m b.g.l. The intrusives are expected to enhance the thermal conditions of the well, improving the general output. However, temperature logs after a heating-up period of 625 days show that the bottom hole temperature is just slightly above  $210^{\circ}\text{C}$ . This indicates that the dyke systems have cooled off, and thus, their contribution to the thermal regime is minimal while the larger granitic intrusion is cooling more gradually.

A comparison between alteration temperature and heating-up profiles indicates an average cooling of close to 70°C. The heating-up profile is assumed to be representative of the formation temperature of the well due to the long duration of the recovery period. Plotting of the boiling curve with depth shows that the geothermal fluids are mainly liquid dominated. Shallow alteration above the boiling curve, that is, from the surface to 900 m b.g.l., indicates that the water level in the past was higher than the current levels of slightly below 400 m b.g.l.

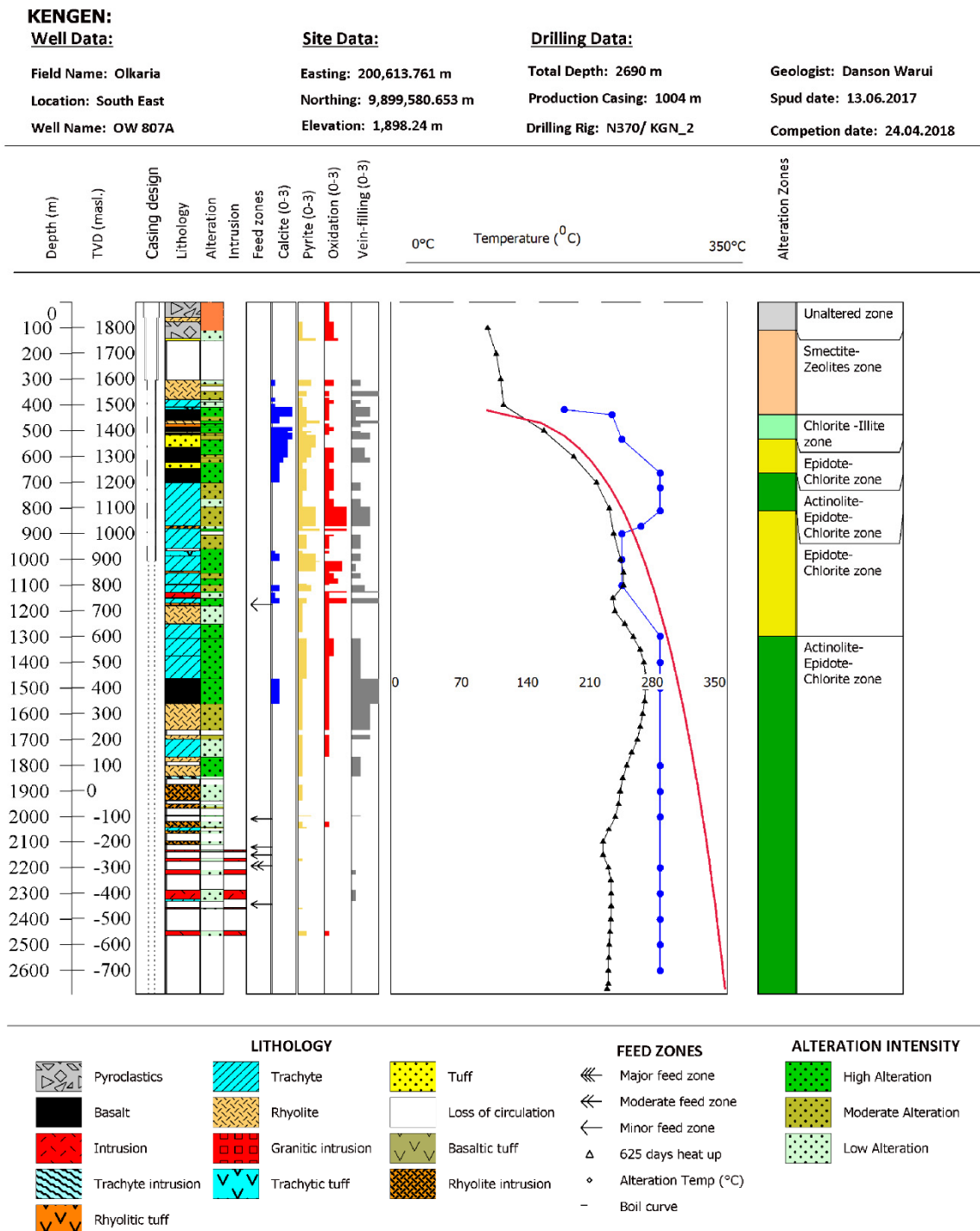


FIGURE 17: Temperature and alteration comparison for well OW-807A

## 5. DISCUSSION

Analysis of the lithology of well OW- 807A conforms to the established lithostratigraphy of the Greater Olkaria Geothermal System where the lithological units have been categorised based on their position, age and tectono-stratigraphy. The well is characterised by four lithostratigraphic units from the surface to the bottom of the well, namely the pyroclastics, Olkaria Rhyolites, which are collectively termed the Upper Olkaria Volcanics, the Olkaria Basalts and the Plateau Trachytes. Intrusions occur at depth and are mainly granitic in composition. The comendites, occurring in the upper zone of the well, show low to moderate alteration intensities and their permeability is associated with joints and fractures. The Olkaria Basalts, due to the abundant clay and calcite, are relatively impermeable, thus forming a suitable caprock for the geothermal system.

The Plateau Trachytes, which are sub-divided into two generic categories based on their texture, that is, into aphyric and the phyrlic (highly porphyritic) types, show varied intensities of alteration ranging from moderate to high, though the aphyric trachytes are more readily altered by the circulating hydrothermal fluids. The Plateau Trachytes are characterised by matrix porosity as well as secondary porosity from fracturing and veining. The permeability varies with depth as can be observed in the varying alteration intensities. The alteration intensity is moderate from depths of 700 m to 900 m b.g.l. and high below. Permeability indicators, such as vein-filling and pyrite, are abundant across these depths, thus making the unit likely to be a suitable reservoir host rock.

The intersection of the granite intrusive with numerous wells within the southeast and the east field at varying depths has led to the hypothesis that it occurs as a 'batholith', yet not *sensu strictissimo*. Further geophysical and petrochemistry studies are necessary to fully understand the extent of this intrusion and its relationship with the thin intrusions encountered in wells in this area. This could provide more data which can possibly be correlated with the series of dykes and volcanic plugs exposed along the profile of the Ol Njorowa Gorge. Current drilling activities in Olkaria have not fully penetrated this igneous body as drilling is usually terminated when it is encountered since its permeability is definitely very low even though the body is associated with higher temperatures.

The hydrothermal alteration mineral zone indicates that OW-807A is characterised by prograde alteration. The shallow part of the well is characterised by smectites and zeolites, indicating low temperatures associated with circulating geothermal fluids. Mordenite, a zeolite mainly associated with highly felsic rocks, is observed in the well. The mineral occurs as deposition in vesicles and vugs, representing temperature conditions of below 100°C (Harvey and Browne, 1991). Occurrence of secondary quartz indicates that the fluids circulating within the well have reached temperatures of up to 180°C. At progressively higher temperatures, chlorite clays form, indicating temperatures of 230°C. Based on the analysis from the SEM composition data, the chlorites analysed from this well indicate an enrichment in Fe<sup>3+</sup> ions. Also, analysis of the diffraction patterns from the XRD analysis of the OW-807A well shows a well-defined peak at d (002) which is higher than the peak at d (001) for chlorite, an indication of the enrichment of Fe<sup>3+</sup> ions in the clay (Moore and Reynolds, 1997).

The precipitation of epidote in OW-807A indicates that the reservoir conditions have attained temperatures of 240°C to 260°C and remain stable with increasing temperatures (Reyes, 1990). The epidote in the upper parts of the well mainly shows the characteristic pistachio-green colour while at depths below 1400 m b.g.l. it changes to a deeper green coloration. This coloration results from changes in Fe<sup>3+</sup> content (Bird et al., 1984). Further increase in temperature allows for the alteration of ferromagnesian minerals into actinolite, which indicates reservoir conditions of between 280°C and 300°C (Browne, 1978). The relatively shallow depths of epidote and actinolite, that is 532 m b.g.l. and 664 m b.g.l., respectively, indicate that the well intersects an up-flow zone in its upper parts. The high temperature plume is responsible for the alteration in the upper parts, while at depth, the deviated well encounters a geothermal convective system.

Mineral sequences in veins and vesicle fillings also indicate the varying temperature conditions with time which enable the precipitation of a higher alteration rank mineral in a similar location. Observations include the infilling of veins and vesicles with clays and quartz, quartz and epidote, as well as quartz and actinolite, indicating the evolution of the thermal regime of the circulating fluids.

However, at a depth range between 982 and 1484 m, secondary fluorite is observed imprinting over earlier quartz and epidote, indicating changes in the thermal conditions. Secondary fluorite is associated with temperatures of 100-150°C and is precipitated as a result of cooler fluid incursions. The deposition of secondary fluorite is a result of an interplay of factors though and studies show that it may be due to changes in temperature and pressure, due to fluid mixing, or it can be a result of fluid-wall rock interactions (Richardson and Holland, 1979). The most plausible mechanism for the deposition of fluorite as a secondary mineral in OW-807A, is inferred to be temperature changes, caused by the mixing of the hot rising geothermal fluids with cooler fluids of meteoric origin. This mixing is believed to occur in the highly permeable NE-SW trending normal faults which are generally dipping to the east and are associated with the Ol Njorowa Gorge. The well intersects these structures below 900 m b.g.l. and the major feed zone at 1150 m b.g.l. occurs within this fault zone. The lithology in this zone is characterised by highly oxidised trachytes, showing abundant vein filling. Calcite and pyrite are also abundant within this zone, further attesting to the highly permeable conditions in this zone. The highly permeable fault zone is characterised by the inflow of cold fluids directly into the reservoir, causing massive temperature reversals within the well.

The analysis of clays in the OW-807A well confirms the occurrence of smectites, mixed layer clays, illite and chlorite clays. Smectite clays are generally categorised as either dioctahedral or trioctahedral sub-groups. They are formed as products of hydrolysis reactions of silicate phases such as volcanic glass, feldspars, olivine, pyroxene and generally represent temperatures below 200°C (Fulignati, 2020). They are mainly found in the shallow zones of the well representative of the low temperatures associated with the circulating geothermal fluids. The mixed layer clays are also common in the study well, marking the transformation of low temperature clays to higher order clays. Within the larger Olkaria geothermal system, the occurrence of mixed layer clays signifies reservoir temperatures of between 200 and 220°C and they represent thermodynamically metastable phases. With increase in temperature, the transformation results in chlorite and illite clays. The occurrence of hydrothermal illite in Olkaria signifies temperatures of above 200°C while chlorite signifies 220°C and the composition variations are highly related to the formation temperature (Fulignati, 2020). Common minerals associated with these clays at these temperatures include epidote, adularia, albite, and prehnite, indicative of the enhanced alteration temperatures within the geothermal system. The occurrence of a type of clay characterised by a  $d(001)$  spacing of 12.3 Å to 12.4 Å which shows no changes due to glycolation, but shows a reduced intensity when heated to 550°C, is interpreted to represent a form of randomly interstratified chlorite-illite clay. SEM analysis of clays at 982 m b.g.l. indicate the presence of interstratified illite and chlorites, though further analysis is required before assigning these clays.

Temperature calculations, based on the application of chlorite clays as possible geothermometers for this part of the field, show temperatures from 191°C to 321°C. Most of the calculated temperatures however range between 247 and 269°C and are interpreted to relate to the current thermal conditions in the well. This shows that the paleo and present thermal conditions are in equilibrium in this depth. However, considerations of the implications of the variability in the substitutions in the chlorite structure are necessary. Comparisons with other methods, such as fluid inclusion analysis, will greatly improve the calibration of this method for this field.

Within permeable sections of the well, a wide range of alteration mineral assemblages are observed. This reflects the ease with which the fluids and rock interactions occurred, resulting in the mobilisation, precipitation and leaching of elements necessary for the formation of these minerals.

## 6. CONCLUSIONS

Studies of the OW-807A well show that it intersects two distinct hydrothermal systems. The upper section is located in the fringes of an up-flow zone. This is indicated by the shallow occurrence of high temperature alteration minerals such as epidote and actinolite, representing thermal conditions above 240°C and 280°C, respectively. The deeper sections penetrate a deep convective system, since the well is deviated away from the established up-flow zone.

The aim of targeting the well towards the dyke systems and volcanic centres in the Ol Njorowa Gorge was to appraise the suitability of these systems as potential heat sources for targeting of production wells. The numerous fault systems were expected to provide permeable zones yielding good well permeability. The study shows that, though the intersection of the permeable zones and the dykes was attained, the faults are characterised by high downflows of cold fluids and the dykes have cooled off relatively, with bottom hole temperatures of around 210°C. This therefore makes them unsuitable for future targeting as potential production wells, but they may be potential targets for direct use or hot re-injection.

Based on the outcome of this study, the following recommendations are made:

- It is necessary to fully analyse the thermal characteristics of other wells targeted towards the Ol Njorowa Gorge and define the sub-surface extent of its zone of influence through fluid inclusion studies.
- There is need to characterise and model the surface of the granitic intrusion intersected by wells in the East and Southeast sectors of the Olkaria Geothermal Field.
- Further studies on the clay's composition and structure in the Olkaria Geothermal Field should be undertaken to fully characterise their chemistry and formation conditions.

## ACKNOWLEDGEMENTS

I take this opportunity to express my sincere gratitude to the Government of Iceland and the GRÓ Geothermal Training Programme (GRÓ GTP) for the fellowship award and my employer Kenya Electricity Generating Company PLC (KenGen) for granting me study leave to attend the course. Special thanks to the Director of GRÓ GTP, Guðni Axelsson, Deputy Director, Ingimar G. Haraldsson, Málfríður Ómarsdóttir, Vigdís Harðardóttir and Markús A.G. Wilde for their unwavering guidance and support throughout the study period.

Special thanks to my supervisors Anette K. Mortensen and Helga Margrét Helgadóttir for their dedication and support during the training and the project work, always putting up with long hours so that the project work remained on course. Anette, the field trips were always a welcome variation from the busy schedules. Your guidance and useful insights have truly made me a better geologist. To Sigurður Sveinn Jónsson, the discussions on the principles of XRD data analysis will always be appreciated. To the staff of ISOR, thank you for taking your time to share your expertise.

Lastly, I extend my sincere appreciation to my dear wife Vallary for taking care of our beloved daughter Valeria during my absence. Thank you.

## REFERENCES

- Achauer, U., Maguire, P.K.H., Mechie, J., and Green, W.V., 1992: Some remarks on the structure and geodynamics of the Kenya Rift. *Tectonophysics*, 213(1), 257–268.
- Albee, A.L., 1962: Relationships between the mineral association, chemical composition and physical properties of the chlorite series. *American Mineralogist*, 47, 851-870.
- Baker, B.H., Mitchell, J.G., and Williams, L.A.J., 1988: Stratigraphy, geochronology and volcano-tectonic evolution of the Naivasha-Kinangop region, Gregory Rift Valley, Kenya. *Journal of the Geological Society*, 145(1), 107-116.
- Battaglia, S., 2004: Variations in the chemical composition of illite from five geothermal fields: a possible geothermometer. *Clay Minerals*, 39, 501-510
- Bird, D.K., Schiffman, P., Elders, W.A., Williams, A.E., and McDowell, S.D., 1984: Calc-silicate mineralization in active geothermal systems. *Economic geology*, 79, 671-695.
- Böðvarsson, G.S., Pruess K., Stefánson V., Björnsson S., and Ojiambo S.B., 1987: East Olkaria geothermal field, Kenya – History match with production and pressure decline data. *J. Geophys. Res.*, 92(B1), 521-539.
- Browne, P.R.L., 1970: Hydrothermal alteration as an aid in investigating geothermal fields. *Geothermics*, 2, 564–570.
- Browne, P.R.L., 1978: Hydrothermal alteration in active geothermal fields. *Annual Reviews of Earth and Planetary Science*, 6, 229-250.
- Browne, P.R.L., 1984a: Subsurface stratigraphy and hydrothermal alteration of the eastern section of the Olkaria geothermal field, Kenya. *Proceedings of the 5th New Zealand Geothermal workshop, Geothermal Institute, Auckland*, 33-41.
- Browne, P.R.L., 1984b: *Lectures on geothermal geology and petrology*. UNU-GTP, Reykjavík, Iceland, report 2, 92 pp.
- Cathelineau, M. 1988: Cation site occupancy in chlorites and illites as a function of temperature. *Clay Miner.*, 23, 471–485.
- Chorowicz, J., 2005: The East African Rift System. *J. African Earth Sciences*, 43, 379-410.
- Clarke, M.C.G., Woodhall, D.G., Allen, D., and Darling G., 1990: *Geological, volcanological and hydrogeological controls on the occurrence of geothermal activity in the area surrounding Lake Naivasha, Kenya, with coloured 1:100 000 geological maps*. Ministry of Energy, Nairobi, 138 pp.
- Deer, W.A., Howie, R.A. and Zussman, J., 1992: *An introduction to the rock-forming minerals* (2<sup>nd</sup> ed.). Longman Scientific and Technical, Hong Kong, 696 pp.
- Ebinger, C.J., Deino, A.L., Drake, R.E and Tesha, A.L., 1989: Chronology of volcanism and rift basin propagation: Rungwe Volcanic province, East Africa. *J. Geophys. Res.*, 94, 15,785-15,803.
- Fulignati, P., 2020: Clay minerals in hydrothermal systems. *Minerals 2020*, 10, 17 pp.



Hackman, B.D., Charsley, T.J., Key, R.M., and Wilkinson, A.F., 1990: The development of the East African Rift System in north- central Kenya. *Tectonophysics*, 184(2), 189-211.

Harvey, C.C., and Browne, P.R.L., 1991: Mixed-layer clay geothermometry in the Wairakei geothermal field, New Zealand. *Clays and Clay Minerals*, 39, 614–621.

Haukwa, C.B., 1984: *Recent measurements within Olkaria East and West fields*. Kenya Power Co., internal report, 13 pp.

Hillier, S., and Velde, B., 1991: Octahedral Occupancy and the chemical composition of diagenetic (low temperature) chlorites. *Clay Minerals*, 26, 149-168.

Hower, J. and Mowatt, T.C., 1966: The mineralogy of illites and mixed- layer illite-montmorillonites. *Amer. Mineral.*, 51, 825-854.

Inoue, A., and Utada, M., 1991: Smectite- to- Chlorite transformation in thermally metamorphosed volcanoclastic rocks in the Kamikita area, northern Honshu, Japan. *American Mineralogist*, 76, 628-640.

Karingithi, C.W., Arnórsson, S., and Grönvold, K., 2010: Processes controlling aquifer fluid compositions in the Olkaria geothermal system, Kenya. *J. Volc. Geothermal Res.*, 196(1), 57-76.

Lagat, J.K., 2004: *Geology, hydrothermal alteration and fluid inclusion studies of the Olkaria Domes geothermal field, Kenya*. University of Iceland, M.Sc. thesis, UNU-GTP, Iceland, report 1, 79 pp.

Lagat, J.K., 2010: Hydrothermal alteration mineralogy in geothermal fields with case examples from Olkaria Domes geothermal field, Kenya. *Presented at "Short Course V on Surface Exploration for Geothermal Resources"*, organized by UNU-GTP, KenGen and GDC at Lake Naivasha, Kenya, 24 pp.

Macdonald, R., Davies, G.R., Bliss, C.M., Leat, P.T., Bailey, D.K., and Smith, R.L., 1987: Geochemistry of high silica peralkaline rhyolites, Naivasha, Kenya rift valley. *Journal of Petrology*, 28, 979-1008.

MacDonald, R., and Scaillet, B., 2006: The central Kenya peralkaline province: insights into the evolution of peralkaline salic magmas. *Lithos*, 91, 59-73.

Mechie, J., Keller, G.R., Prodehl, C., Khan, M.A., and Gaciri, S.J., 1997: A model for the structure, composition and evolution of the Kenya rift. *Tectonophysics*, 278, 95–119.

Meunier, A., 2005: *Clays*. Springer, Berlin, Germany, 472 pp.

Moore, D.M., and Reynolds, R.C., 1997: *X-Ray diffraction and the identification and analysis of clay minerals* (2<sup>nd</sup> edition). Oxford University Press, New York, 378 pp.

Muchemi, G.G., 1992: *Structural map of Olkaria geothermal field showing inferred ring structures*. Kenya Power Company, internal report, 22 pp.

Muchemi, G.G., 2000: *Conceptualized model of Olkaria geothermal field*. Kenya Electricity Generating Company PLC, internal report, 13 pp.

Munyiri, S.K., 2016: *Structural mapping of Olkaria Domes Geothermal Field using geochemical soil gas surveys, remote sensing and GIS*. Faculty of Earth Sciences, University of Iceland, MSc thesis, UNU-GTP, report 5, 64 pp.

Naylor, W.I., 1972: *Geology of the Eburru and Olkaria prospects*. U.N. Geothermal Exploration Project, report, 104 pp.

Omenda, P.A., 1998: The geology and structural controls of the Olkaria geothermal system, Kenya. *Geothermics*, 27(1), 55-74.

Otieno, V.O., 2016: *Borehole geology and sub-surface petrochemistry of the Domes area, Olkaria geothermal field, Kenya, in relation to well OW-922*. Faculty of Earth Science, University of Iceland, MSc thesis, UNU-GTP, report 2, 84 pp.

Reed, S.J.B., 2005: *Electron microprobe analysis and scanning electron microscopy in geology: 2nd ed.* Cambridge, New York, Melbourne: Cambridge University Press. xiii + 192 pp.

Reyes, A.G., 1990: Petrology of Philippine geothermal systems and the application of alteration mineralogy to their assessment. *J. Volc. Geoth. Res.*, 43, 279-309.

Richardson, C.K., and Holland, H.D., 1979: Fluorite deposition in hydrothermal systems. *Geochimica et Cosmochimica Acta*, 43(8), 1327-1335.

Rogers, N., Macdonald, R., Fitton, J.G., George, R., Smith, M., and Barreiro, B., 2000: Two mantle plumes beneath the East African rift system: Sr, Nd and Pb isotope evidence from Kenya Rift basalts. *Earth and Planetary Science Letters*, 176, 387-400.

Shanks III, W.C.P., 2012: Hydrothermal alteration (Chapter 11). In: Shanks III, W.C.P. and Thurston, R. (eds.), *Volcanogenic massive sulfide occurrence model*. U.S. Geological Survey, Reston, Virginia, 363 pp.

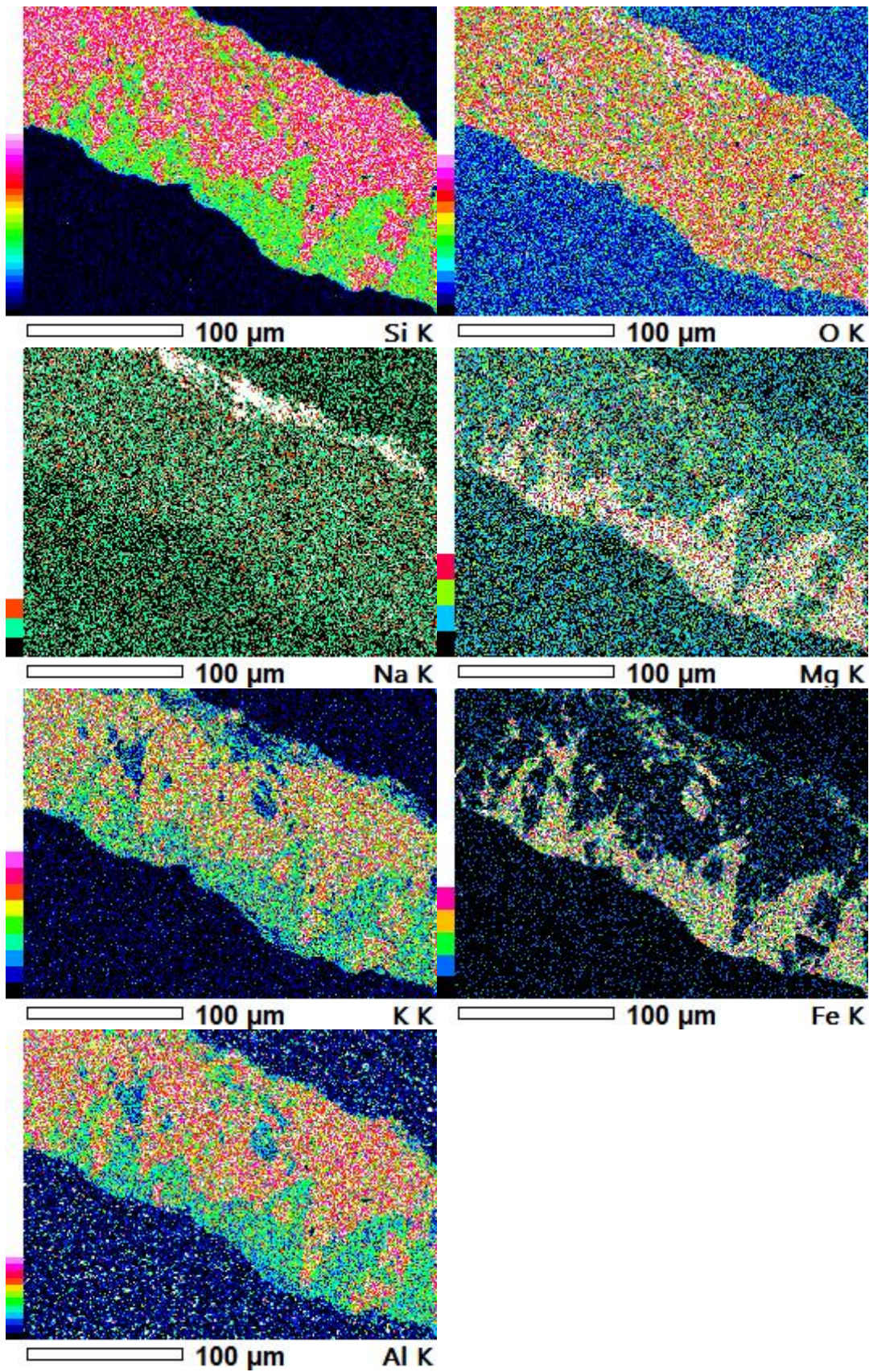
Smith, M., and Mosley, P., 1993: Crustal heterogeneity and basement influence on the development of the Kenya rift, East Africa. *Tectonics*, 12, 591-606.

Steiner, A., 1968: Clay minerals in hydrothermally altered rocks at Wairakei, New Zealand. *Clays and Clay Minerals*, 16, 193-213.

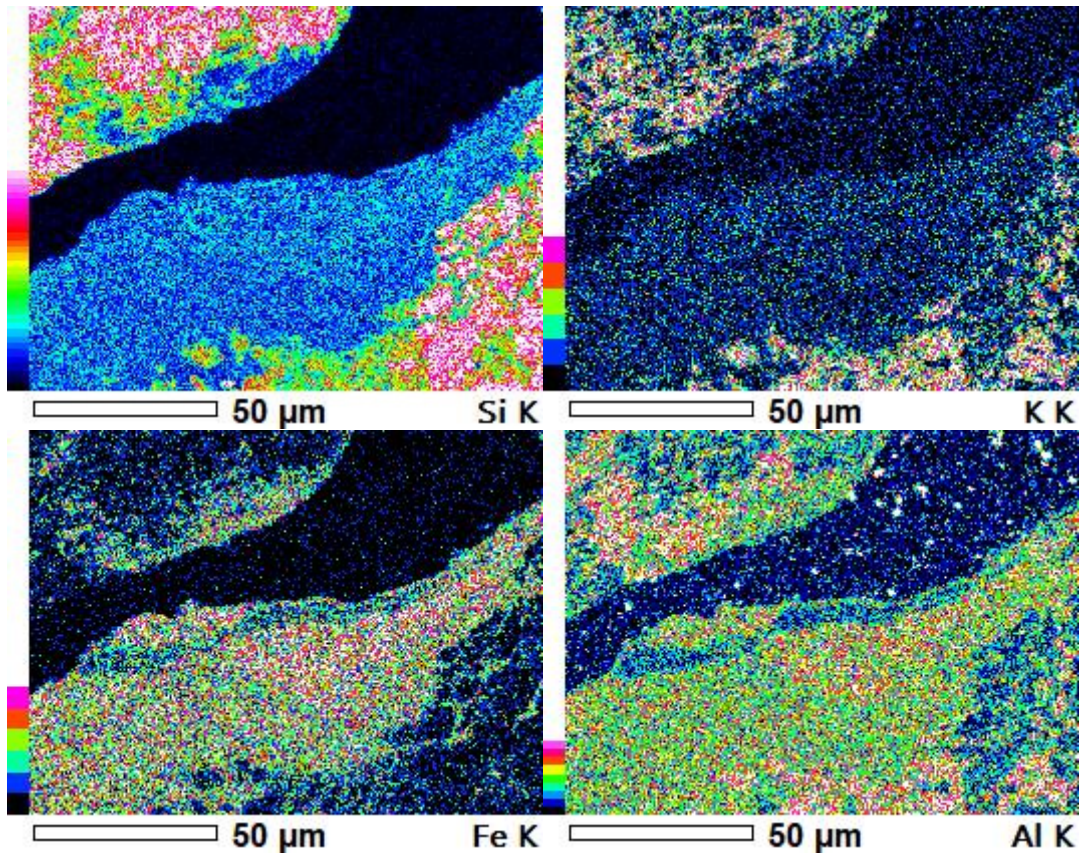
Strecker, M.R., Blisniuk, P.M., and Eisbacher, G.H., 1990: Rotation of extension direction in the Central Kenyan Rift. *Geology*, 18, 299-302.

Yavuz, F., Kumral, M., Karakaya, N., Karakaya C.M., and Yildirim, K.D., 2015: A Windows program for chlorite calculation and classification. *Computers and Geosciences*, 81, 101-113.

**APPENDIX 1:** Elemental compositional maps of Illite clays at 1480 m b.g.l.

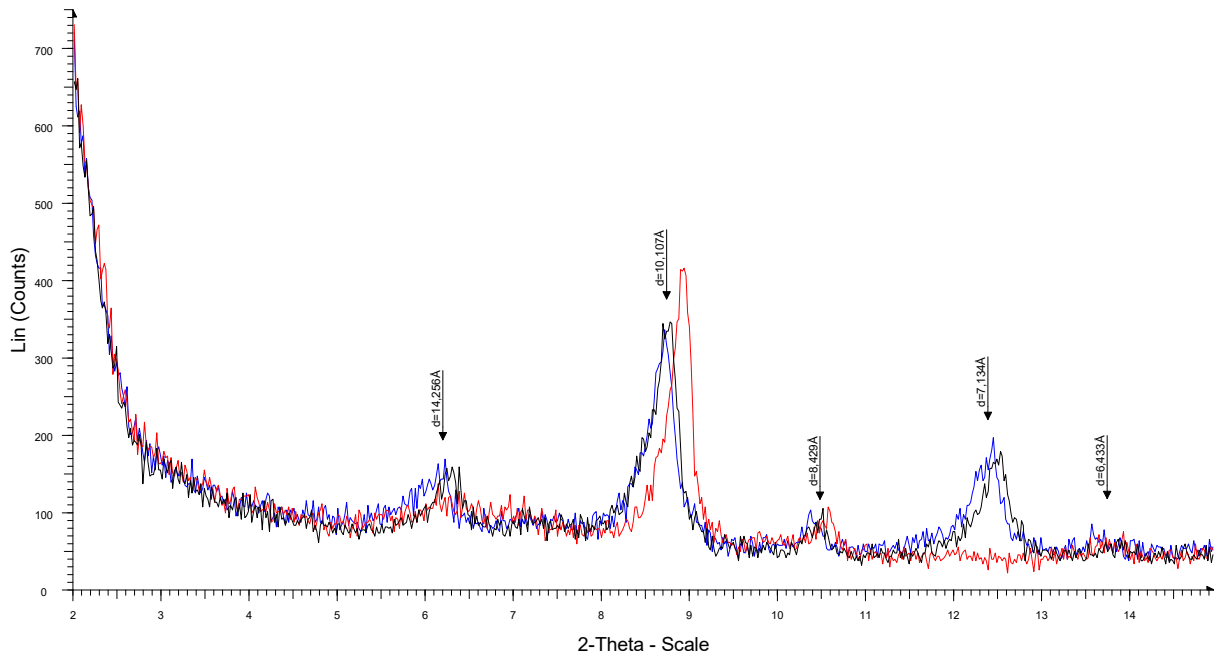


**APPENDIX 2:** Elemental composition maps of chlorite at 982 m b.g.l.



## APPENDIX 3: XRD diffractograms for chlorite and illite in well OW-807A

## OW-807A 1480-1484 m



File: 1480-1484A\_1.raw - Type: 2Th/Th locked - Start: 2.000 ° - End: 14.960 ° - Step: 0.020 ° - Anode: Cu - WL1: 1.54056 - Generator kV: 36 kV - Generator mA: 36 mA - Company: File created with PowDLL Nikos  
File: 1480-1484G\_1.raw - Type: 2Th/Th locked - Start: 2.000 ° - End: 14.960 ° - Step: 0.020 ° - Anode: Cu - WL1: 1.54056 - Generator kV: 36 kV - Generator mA: 36 mA - Company: File created with PowDLL Nikos  
File: 1480-1484H\_1.raw - Type: 2Th/Th locked - Start: 2.000 ° - End: 14.960 ° - Step: 0.020 ° - Anode: Cu - WL1: 1.54056 - Generator kV: 36 kV - Generator mA: 36 mA - Company: File created with PowDLL Nikos